

# 2D ANALYSIS OF A STRATEGIC STRUCTURE SUBJECTED TO BLAST LOADS

## A DISSERTATION

*submitted in partial fulfilment of the  
requirements for the award of the degree*

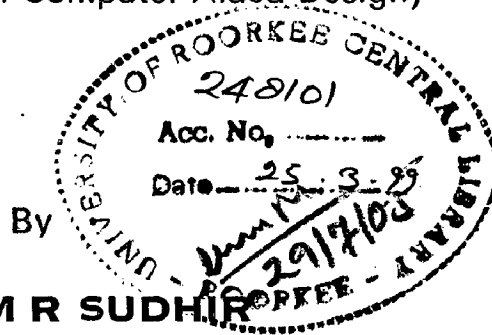
*of*

MASTER OF ENGINEERING

*in*

CIVIL ENGINEERING

(With Specialization in Computer Aided Design)



MAJOR M R SUDHIR



DEPARTMENT OF CIVIL ENGINEERING  
UNIVERSITY OF ROORKEE  
ROORKEE-247 667 (INDIA)


JANUARY, 1998

# CANDIDATE'S DECLARATION

I hereby certify that the work which is being presented in this dissertation entitled "2D ANALYSIS OF A STRATEGIC STRUCTURE SUBJECTED TO BLAST LOADS" in partial fulfilment of the requirements for the award of degree of MASTER OF ENGINEERING with specialisation in COMPUTER AIDED DESIGN, submitted in the Department of Civil Engineering, University of Roorkee, Roorkee, India is an authentic record of my own work carried out during the period from July 1997 to January 1998, under the supervision of Dr P N Godbole, Professor, Department of Civil Engineering, University of Roorkee, Roorkee, India.

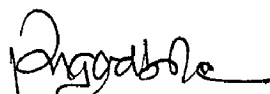
I further state that the matter embodied in this dissertation has not been submitted by me for the award of any other degree or diploma of this or any other university.

Date: 28 Jan 1998

  
(M R SUDHIR)  
MAJOR

This is to certify that the above statement made by the candidate is correct to the best of my knowledge.

Date: 27, Jan 1998

  
(Dr P N Godbole)  
Professor  
Dept. of Civil Engineering  
University of Roorkee  
Roorkee - 247667, India

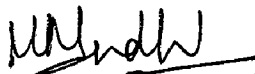
# ACKNOWLEDGEMENT

I express my sincere gratitude to **Dr P N Godbole**, Professor, Department of Civil Engineering, University of Roorkee for guiding me through this dissertation work. His guidance, advice and encouragement throughout this work was invaluable.

I also wish to express my gratitude to **Mr Sanjeev Kumar Garg**, Senior Research Fellow for his guidance, constant advice and keen interest throughout the work.

Finally, the consistent moral support extended by my wife, **Suma** and my daughter, **Shraddha** deserves a special mention.

Date: 28 Jan 1998

  
(M R SUDHIR)  
MAJOR

# ABSTRACT

The inherent strength of a bunker makes it an effective blast resistant structure. Strategic structures like bunkers are used for the protection of personnel, equipment and for storage of explosives/ammunition.

Explosive blasts exert loads of high intensity and short duration on structures in the vicinity of the blast. Explosives even from small charges when placed close to a structure would result in very high peak pressures and could lead to damage.

In this dissertation work, two dimensional analysis of bunkers subjected to blast loads has been carried out. Non-linear transient dynamic analysis for blast loads has been carried out by the general purpose finite element program which includes the numerically integrated isoparametric elements. In the elasto-plastic analysis, Tresca, Von Mises, Mohr-Coulomb and Drucker-Prager yield criteria have been considered.

An above ground bunker, a bunker with soil cover and a semi-buried bunker have been analysed for blast loads as recommended by IS:4991-1968.

# CONTENTS

	<b>Page No.</b>
CANDIDATE'S DECLARATION	(i)
ACKNOWLEDGEMENT	(ii)
ABSTRACT	(iii)
LIST OF FIGURES	(vii)
CHAPTER 1	
INTRODUCTION	1
1.1    General	1
1.2    The Concept of Blast Loads	1
1.3    Review of Certain Earlier Work	2
1.4    Elasto-Plastic Finite Element Analysis	3
1.5    Objectives of the Present Study	3
1.6    Organisation of Work	4
CHAPTER 2	
BLAST LOADS	5
2.1    Introduction	5
2.2    Various Codes and Specifications	5
2.3    Classification of Blast Loads	6
2.3.1 Unconfined explosions	6
2.3.2 Confined explosions	8
2.4    Blast Hazards to Bunkers	9
2.5    Blast Load Calculations and Pressure-Time Curves	10
2.5.1 Case A	10
2.5.2 Case B	12
2.5.3 Case C	13

CHAPTER 3	NON LINEAR TRANSIENT DYNAMIC ANALYSIS	15
3.1	Introduction	15
3.2	Dynamic Equilibrium Equation	15
3.3	Implicit Time Schemes	17
	3.3.1 New mark's algorithm	17
	3.3.2 Predictor-corrector algorithm	19
3.4	Implicit-Explicit Algorithms	20
CHAPTER 4	ELASTO-PLASTIC FINITE ELEMENT ANALYSIS	23
4.1	Introduction	23
4.2	Preliminary Theory for Two Dimensional Elasto-Plastic Applications	24
4.3	Linear Elastic Constitutive Matrix for Plane Stress, Plane Strain and Axisymmetric Cases	24
	4.3.1 Plane stress problems	24
	4.3.2 Plane strain problems	25
	4.3.3 Axisymmetric problems	25
4.4	Isoparametric Finite Element Representation	26
	4.4.1 Jacobian matrix	27
	4.4.2 Stiffness matrix of the element	29
4.5	Two Dimensional Elasto-Plastic Problems	30
	4.5.1 Introduction	30
	4.5.2 The mathematical theory of plasticity	31
	4.5.3 General form of yield criteria	31
	4.5.4 Work or strain hardening	35
	4.5.5 Elasto-plastic stress-strain relation	36

	4.5.6 The yield criteria for numerical computation	37
	4.5.7 The yield criteria	39
	4.5.8 The flow vector for numerical computation	40
	4.5.9 Singular points on the yield surface	42
CHAPTER 5	CASE STUDIES	44
	5.1 Introduction	44
	5.2 Features of Computer Program	44
	5.3 Types of Bunkers Considered for Analysis	45
	5.4 The Problem Definition	45
	5.4.1 An above ground bunker	45
	5.4.2 A bunker with soil cover	45
	5.4.3 Semi-buried bunkers	45
	5.5 The Blast Loads on the Bunkers	46
	5.6 Results and Discussions	46
	5.6.1 The geometry of problem	46
	5.6.2 Boundary conditions	46
	5.6.3 Loading conditions	46
	5.6.4 Material parameters	47
	5.6.5 Discussions	47
CHAPTER 6	CONCLUSIONS	49
FIGURES		51
TABLES		82
REFERENCES		84

## LIST OF FIGURES

Figure Number	Particulars	Page No.
2.1	Free-Air Burst Environment	51
2.2	Positive Phase Shock Wave Parameters for A Spherical TNT Explosion in Free Air at Sea Level	52
2.3	Air Burst Environment	53
2.4	Variation of Reflected Pressure as a Function of Angle of Incidence	54
2.5	Variation of Scaled Reflected Impulse As a Function of Angle of Incidence	55
2.6	Surface Burst Blast Environment	56
2.7	Positive Phase Shock Wave Parameters for a Hemispherical TNT Explosion on the Surface at Sea Level	57
2.8	Pressure-Time Curve for 100 kg Explosive at 20 m Distance - Front Face Loading	58
2.9	Pressure-Time Curve for 100 kg Explosive at 20 m Distance - Roof Loading	58
2.10	Pressure -Time Curve for 30 kg Explosive at 10 m Distance - Front Face Loading	59
2.11	Pressure - Time Curve for 30 kg Explosive at 10 m Distance -Roof Loading	59
2.12	Pressure - Time Curve for 10 kg Explosive at 5 m Distance - Front Face Loading	60
2.13	Pressure - Time Curve for 10 kg Explosive at 5 m Distance - Roof Loading	60
4.1	Geometrical Representation of the Tresca and Von Mises Yield Surfaces in Principal Stress Space	61



4.2	Two Dimensional Representations of the Tresca and Von Mises Yield Criteria	61
4.3	Mohr Circle Representation of the Mohr-Coulomb Yield Criterion	62
4.4	Geometrical and $\pi$ Plane Representation of the Mohr-Coulomb and Drucker-Prager Yield Criteria	62
4.5	Mathematical Models for Representation of Strain Hardening Behaviour	63
5.1	Above Ground Bunker	64
5.2	Above Ground Bunker with Soil Cover	65
5.3	Semi-Buried Bunker	66
5.4	Response of an Above Ground Bunker for 100 kg Explosive at 20 m Distance	67
5.5	Response of an Above Ground Bunker for 30 kg Explosive at 10 m Distance	68
5.6	Response of An Above Ground Bunker For 10 kg Explosive at 5 m Distance	69
5.7	Response of an Above Ground Bunker with Soil Cover for 100 kg Explosive at 20 m Distance	70
5.8	Response of an Above Ground Bunker with Soil Cover for 30 kg Explosive at 10 m Distance	71
5.9	Response of an Above Ground Bunker with Soil Cover for 10 kg Explosive at 5 m Distance	72
5.10	Response of a Semi-Buried Bunker for 100 kg Explosive at 20 m Distance	73
5.11	Response of a Semi-Buried Bunker for 30 kg Explosive at 10 m Distance	74
5.12	Response of a Semi-Buried Bunker for 10 kg Explosive at 5 m Distance	75
5.13	Deflected Profile of an Above Ground Bunker at Various Time intervals	76

5.14	Deflected Profile of an Above Ground Bunker with Soil Cover at Various Time intervals	77
5.15	Deflected Profile of a Semi-Buried Bunker at Various Time intervals	78
5.16	Yielded Profile of an Above Ground Bunker	79
5.17	Yielded Profile of an Above Ground Bunker with Soil Cover	80
5.18	Flow chart of computer program	81

# CHAPTER 1

## INTRODUCTION

### 1.1 GENERAL

Strategic structures like bunkers are an integral part of the defensive battle plan. They are used for the protection of personnel, equipment and for storage of explosives/ammunition. With the ever increasing sophistication of weapons, there is a specific need to have bunkers which can withstand heavy blast loads. One of the main lessons of the Gulf war was that the underground bunkers provide excellent protection even against air bombardments and artillery shelling. The blast pressures are of high intensity and short duration, which damage structures in the vicinity, destroy equipment and personnel. Thus the knowledge of bunker's response to blast loads has become extremely important in military applications.

### 1.2 THE CONCEPT OF BLAST LOADS

Explosives when detonated on or above ground, results in a very rapid release of large amounts of energy within a short time, thus generating a pressure wave in the surrounding medium known as a shock wave. The shock wave has a sudden increase in pressure at the front known as shock front. The shock front expands outwards from the surface of the explosive into the surrounding air. As the wave expands, it decays in strength, lengthens in duration and decreases in velocity. As the wave expands in air, the front impinges on the structure located within its path and then the entire structure is engulfed by the shock pressure.

When the shock front strikes an object such as building, (2) there is a diffraction effect producing forces which result from the higher pressures due to reflection of the wave on the front face of the object and also from the time lag

before the overpressure acts on the rear face. At the same time, the air behind the shock front is moving outward at high velocity and this wind produces drag forces on any objects encountered. Thus the total loading consists of three parts:

- (a) The incident overpressure
- (b) The reflected pressure
- (c) The drag pressure due to blast wind.

### **1.3 REVIEW OF CERTAIN EARLIER WORK**

Although there seems to be a lot work going on in the field of blast loads, very little information is available on the subject as the subject matter has been categorised as classified. However, certain Research papers and Thesis work which are available for reference have been mentioned here. A Research paper on Analysis of blast loaded buried RC Arch response, has been published (10,11). In this, two shallow buried reinforced concrete arches that were blast loaded (using explosive generated pressures applied to the soil surface) in separate test programs have been analysed. The geometry and structural detailing of the two specimens are different, as are the soil properties, depths of burial and the surface blast pressures.

A Ph.D. Thesis on Dynamic response of structures subjected to missile impact has been carried out(4). A material model for reinforced concrete suitable for transient dynamic analysis has been presented.

A ME Thesis on computer aided design of RCC box type structures for blast loading has been carried out(7). In this, a CAD software has been developed for the design of RCC Box type structures subjected to blast loading. It calculates blast loads on slabs and has a facility for structural drawing.

A ME Thesis on blast resistance and shatter proof properties of composite elements has been carried out (9). In this, tests on composite elements for

ascertaining their blast resistance and shatter proof properties have been described and results have been presented.

A Ph.D. Thesis on Inelastic dynamic analysis of concrete frames under non-nuclear blast loadings has been carried out (12). The study has been carried out with specific reference to frame structures.

#### **1.4 ELASTO-PLASTIC FINITE ELEMENT ANALYSIS**

The finite element method is now firmly accepted as one of the most powerful general techniques for the numerical solution of a variety of problems encountered in engineering. The technique is widely employed as a design tool for linear and nonlinear analysis. The Elasto-plastic behaviour is characterised by an initial elastic material response onto which a plastic deformation is superimposed after a certain level of stress has been reached. Plastic deformation is essentially irreversible on unloading and is incompressible in nature. The onset of plastic deformation (or yielding) is governed by a yield criterion and the post yield deformation generally occurs at a greatly reduced material stiffness.

#### **1.5 OBJECTIVES OF THE PRESENT STUDY**

The Thesis deals with the two dimensional analysis of bunkers, which are an important class of strategic structures, for the blast loads as specified by the Indian standard code of practice. A non-linear Transient Dynamic analysis of the bunkers has been carried out in the elasto-plastic range using Finite Element Method. For this purpose an available computer program based on the Implicit-Explicit time integration scheme for two dimensional plane stress/plane strain and axisymmetrical non-linear dynamic transient problems (8) has been used.

The objectives of the present study have been:

- (a) To study the behaviour of an above ground bunker, a bunker with soil cover and a semi buried bunker, when subjected to blast loads as recommended by IS code of practice.
- (b) To carry out a parametric study of the blast load effects under three different load intensities and charge-bunker distances.
- (c) To ascertain the requirement of elasto-plastic analysis for bunkers subjected to blast loads.

## **1.6 ORGANISATION OF WORK**

This dissertation work has been divided into six chapters.

Chapter 2 deals with the fundamentals of blast loads. In this, various codes and specification available on the subject, the categories of blast loads to include confined and unconfined explosions and blast load calculations have been described.

Chapter 3 deals with the non-linear transient dynamic analysis. In this dynamic equilibrium equation, Explicit and Implicit schemes, a combined Implicit and Explicit algorithm have been described.

Chapter 4 deals with the elasto-plastic finite element analysis. It describes the fundamentals of elasto-plastic analysis, Isoparametric finite element representation and the four yield criteria considered in elasto-plastic analysis namely Tresca, Von Mises, Mohr-Coulomb and Drucker-Prager criteria.

Chapter 5 primarily deals with the case studies. In this, the effects of IS Code recommended blast loads on an above ground bunker, a bunker with soil cover and a semi-buried bunker have been studied. The results and discussions have also been included in this Chapter.

Chapter 6 summarizes the conclusions drawn from the present study.

# CHAPTER 2

## BLAST LOADS

### 1 INTRODUCTION

The blast responses of the structures have been drawing attention of Engineers and Scientists all over the world in both military and civilian fields. Keeping in mind the sophisticated weapons being used world over, the requirement of strategic structures capable of resisting heavy blast loads need not be overemphasized. As brought out in the Gulf war, the only protection for the Iraqi soldiers and civilian population from the bombings were underground bunkers. Explosive blasts exert loads of high intensity and short duration on structures in the vicinity of blast, leading to its damage and causing damage to equipment and personnel. Thus, the knowledge of structural response under blast loadings is becoming increasingly important in military applications. Explosive manufacturing and storing facilities also require blast resistant structures.

### 2.2 VARIOUS CODES AND SPECIFICATIONS

The various Codes and specifications which describe the blast loads are

- (a) IS Code:4991-1968 Indian Standard criteria for Blast resistant Design of Structures for explosions above ground.
- (b) US Army Special Publication Vol.I to VI, structures to resist the effects of Accidental Explosions.
- (c) A manual for the prediction of Blast and Fragment loadings on Structures by Baker W E.

## **2.3 CLASSIFICATION OF BLAST LOADS**

The Blast loads on structures can be divided into two main groups based on the confinement of the explosive charge as:

- (a) Unconfined explosions
- (b) Confined explosions

The above two can further be subdivided based on the blast loading produced on the structure and the relative charge location. The subdivided categories are free air burst, air burst, surface burst, fully vented explosion, partially confined explosion and fully confined explosion (13 and 14).

### **2.3.1 Unconfined Explosions**

#### **Free air burst**

When a detonation occurs adjacent to and above a protective structure such that no amplification of the initial shock wave occurs between the explosive source and the protective structure, then the blast loads acting on the structure are free air blast pressures. Free air burst environment is as shown Fig.2.1.

As the incident wave moves radially away from the centre of explosion, it impacts on the structure. Upon impact, the initial wave of pressure and impulse is reinforced and reflected. When the shock wave impinges on a surface oriented so that a line which describes the path of travel of the wave is normal to the surface, then the point of initial contact is said to sustain the maximum pressure and impulse. The positive phase pressures, impulses, time durations and other parameters of this shock environment for a spherical TNT explosion are as given in Fig.2.2.



## **Air burst**

The air burst environment is produced by detonations which occur above the ground surface and at a distance away from the protective structure so that the initial shock wave, propagating away from the explosion impinges on the ground surface prior to arrival at the structure. As the shock wave continues to propagate outward along the ground surface, a front known as Mach front is formed by the interaction of the initial wave (incident wave) and the reflected wave. This is as shown in Fig. 2.3.

The height of Mach front increases as the wave propagates away from the centre of detonation. This increase in height is referred to as the path of triple point and is formed by the intersection of the initial, reflected and Mach waves.

In determining the magnitude of air blast loads acting on the surface of an above ground protective structure, the Peak incident blast pressures in the Mach wave acting on the ground surface immediately before the structure are calculated first. The peak incident pressure is determined for this point, using the scaled height of charge above ground  $H_c/W^{1/3}$  and the angle of incidence  $\alpha$ , where  $H_c$  is the charge height and  $W$  is the charge weight. This is obtained from Fig.2.4.

A similar procedure is used to determine the impulse of the blast wave acting on the ground surface immediately before the structure. This is obtained from Fig.2.5. All other blast parameters can be obtained from Fig.2.2.

## **Surface burst**

A charge located very near or on the ground surface is considered to be responsible for a surface burst. The initial wave of the explosion is

reflected and reinforced by the ground surface to produce a reflected wave. The reflected wave merges with the incident wave at the point of detonation to form a single wave, similar in nature to the Mach wave of the air burst but essentially hemispherical in shape as in Fig.2.6. The positive phase parameters of the surface burst environment for hemispherical TNT explosions are represented as in Fig.2.7. A comparison of these parameters with those of free air explosions indicate that, at a given distance from a detonation of the same weight of explosive, all the parameters of surface burst environment are 1.8 times larger than those for the free air environment (1).

### **2.3.2 Confined Explosions**

#### **Effects of confinement**

When an explosion occurs within a structure, the Peak pressures associated with the initial shock front will be extremely high and in turn, will be amplified by their reflections within the structure. In addition, the accumulation of gases from the explosion will exert additional pressures and increase the load duration within the structure. The combined effects of both pressures may eventually destroy the structure unless venting for the gas and the shock pressures is provided. The structures provided with venting will permit the blast wave from an internal explosion to spill over onto the exterior ground surface. These pressures are referred to as leakage or exterior pressures. The pressures reflected and reinforced within the structure are referred to as interior shock front pressures, while those pressures produced by the accumulation of the gaseous products of the explosion are identified as gas pressures.

### **Fully vented explosions**

A fully vented explosion will be produced within or immediately adjacent to a barrier or cubicle type structure with one or more surfaces open to the atmosphere. The initial wave which is amplified by non-frangible portions of the structure and the products of detonation are totally vented to the atmosphere forming a shock wave which propagates away from the structure.

### **Partially confined explosions**

A partially confined explosion will be produced within a barrier or cubicle type structure with limited size openings and/or frangible surfaces. The initial wave which is amplified by the frangible and non-frangible portions of the structure and the products of detonation are vented to the atmosphere after a finite period of time.

### **Fully confined explosions**

Full confinement of an explosion is associated with either total or near total containment of the explosion by a barrier structure. The internal blast loads will consist of unvented shock loads and very long duration gas pressures which are a function of the degree of confinement. The magnitude of leakage pressures will usually be small.

## **2.4 BLAST HAZARDS TO BUNKERS**

Bunkers are exposed to primarily surface bursts which may be due to air attacks, artillery or mortar shelling. Therefore in the present study, an attempt has been made to study the effects of blast of various intensities at different distances on bunkers. As the blast effect is more critical on above ground and semi-buried bunkers, the same have been considered.

IS:4991-1968 recommends blast loads for design of various type of structures which are as in Table 2.1.

However, in the case of Artillery/Mortar fire, the charge weight is much lower than 100 kg but the blast distance may be lesser. Therefore, blast effects of lesser charge weight taking place at a closer distance than those recommended by the IS Code have also been considered.

## 2.5 BLAST LOAD CALCULATIONS AND PRESSURE-TIME CURVES

Three different weights of explosive at varying distance from ground zero to the point under consideration, are used for blast pressure calculations.

### 2.5.1 Case A

In this, 100 kg of explosive is at a distance of 20 m as per table 7 of page 33, IS:4991-1968.

Scaled distance,  $x = \frac{\text{Actual distance}}{(W)^{1/3}}$  where

$W$  is the weight of explosive in tonnes.

$$x = \frac{20}{(0.1)^{1/3}} = 43.089.$$

From table 1, page 10 of IS:4991-1968, for  $x = 43.089$

$$p_{s0}/p_a = \text{Peak side on overpressure} = 0.7237$$

$$M = \text{Mach number} = 1.2691$$

$$t_d = \text{Duration of equivalent triangular pulse} \\ = 20.7082 \text{ milli secs.}$$

$$\text{Actual } t_d = 20.7082 \times W^{1/3} = 9.6119 \text{ ms}$$

Considering  $p_a$ , the ambient air pressure to be  $1 \text{ kg/cm}^2$ ,

$$q_o/p_a = \text{Dynamic pressure ratio} = 0.17$$

$$p_{r0}/p_a = \text{Peak reflected overpressure ratio} = 1.8575$$

$$p_{s0} = 0.7237 \text{ kg/cm}^2$$

$$q_0 = 0.17 \text{ kg/cm}^2$$

$$p_{r0} = 1.8575 \text{ kg/cm}^2$$

Front face loading

$$U = \text{Shock front velocity} = M.a$$

where,

$$a = \text{Velocity of sound in air at MSL} = 344 \text{ m/s}$$

$$M = \text{Mach number}$$

$$U = M.a = 1.2691 \times 344 = 436.57 \text{ m/s}$$

$t_c$  = clearance time is the time in which the reflected over pressure drops from the peak value  $p_{r0}$  to overpressure  $(p_{s0} + C_d q)$ .

$$t_c = \frac{3S}{U} \text{ or } t_d \text{ whichever is less, where}$$

$$S = H \text{ or } B/2 \text{ whichever is less}$$

For the bunker under consideration,

$$L = 2.6 \text{ m, } H = 3.0 \text{ m and } B = \text{Infinity being a plane strain problem.}$$

$$S = H = 3.0 \text{ m.}$$

$$t_c = \left( \frac{3 \times 3}{436.57} \right) \times 10^3 = 206.152 \text{ ms} > t_d$$

As  $t_c > t_d$ ,  $t_c$  is limited to 9.6119 ms.

From Table 2, page 13 of IS:4991-1968,

$$c_d = \text{Drag co-efficient} = 1 \text{ for front face.}$$

$$p_s + c_d q_0 = 0.8937 \text{ kg/cm}^2$$

The pressure time curve for front wall loading is as Fig. 2.8.

## Roof loading

The value of drag co-efficient corresponding to  $q_0 = 0.17 \text{ kg/cm}^2$  from Table 2, page 13 IS:4991-1968 is - 0.4.

$$t_t = \text{transit time} = \frac{L}{U} = \frac{2.6}{4365.7} = 5.956 \text{ ms}$$

$$(p_{s0} + c_d q_0) = (0.7237 + (-0.4 \times 0.17)) = 0.6557 \text{ kg/cm}^2$$

The pressure time curve for roof loading is as shown in Fig.2.9.

### 2.5.2 Case B

Weight of explosive = 30 kgs

Distance = 10 m

$$x = \frac{10}{(0.03)^{1/3}} = 32.183$$

From Table 1, page 10 of IS: 4991 - 1968, for  $x = 32.183$ ,

$$p_{s0}/p_a = 1.255$$

Considering  $p_a = 1 \text{ kg/cm}^2$ ,  $p_{s0} = 1.255 \text{ kg/cm}^2$

$$M = 1.4363$$

$$t_d = 16.0595 \text{ ms}$$

Actual time,  $t_d = 4.9900 \text{ ms}$

$$q_0/p_a = 0.4782, q_0 = 0.4782 \text{ kg/cm}^2$$

$$p_{r0}/p_a = 3.6543, p_{r0} = 3.6543 \text{ kg/cm}^2$$

### Front face loading

$$U = M.a \quad \text{where}$$

$$a = 344 \text{ m/s}$$

$$U = 1.4363 \times 344 = 494.1011 \text{ ms}$$

$$t_c = \frac{3S}{U} \text{ or } t_d \quad \text{whichever is less}$$

where,

$$S = 3.0 \text{ m}$$

$$t_c = \left( \frac{3 \times 3}{494.1011} \right) \times 10^3 = 18.22 \text{ ms}$$

As  $t_c > t_d$ ,  $t_c = t_d = 4.99 \text{ ms}$

For front face loading,  $C_d = 1$

$$p_{s0} + c_d q_0 = 1.7332 \text{ kg/cm}^2$$

The pressure time curve for front face is as shown in Fig.2.10.

### Roof Loading

From Table 2 IS:4991-1968, drag coefficient corresponding to

$$q_0 = 0.4782 \text{ kg/cm}^2 \text{ is } - 0.4$$

$$\text{Transit time, } t_t = \frac{L}{U} = \frac{2.6}{494.1011} \times 10^3 = 5.26 \text{ ms}$$

As  $t_t > t_d$ , the load on roof may be considered as a moving triangular pulse having the peak value of overpressure ( $p_{s0} + c_d q_0$ ) and time  $t_d$  as shown in Fig.2.11.

### 2.5.3 Case C

Weight of explosive = 10 kg.

Distance = 5 m

$$x = \frac{5}{(0.01)^{1/3}} = 23.208$$

From Table 1 IS:4991-1968, for  $x = 23.208$

$$p_{s0}/p_a = 2.6376$$

Considering  $p_a = 1 \text{ kg/cm}^2$ ,  $p_{s0} = 2.6376 \text{ kg/cm}^2$

$$M = 1.8054$$

$$t_d = 10.7210 \text{ ms}$$

$$\text{Actual } t_d = (W)^{1/3} \times 10.7210 = 2.3098 \text{ ms}$$

$$q_0 = 1.8253 \text{ kg/cm}^2$$

Front wall loading

$$c_d = 1$$

$$U = M.a = 621.06 \text{ m/s}$$

$$t_c = \frac{3S}{U} = \frac{3 \times 3}{621.06} = 14.49 \text{ ms}$$

$$\text{As } t_c > t_d, \quad t_c = t_d = 2.3098 \text{ ms}$$

$$p_{s0} + c_d q_0 = 4.4629 \text{ kg/cm}^2$$

The pressure time curve is as shown in Fig.2.12.

### Roof Loading

From Table 2 IS:4991-1968, drag co-efficient corresponding to

$$q_0 = 1.8253 \text{ kg/cm}^2 \quad \text{is } -0.3.$$

$$\text{Transit time, } t_t = \frac{L}{U} = \left( \frac{2.6}{621.06} \right) \times 10^3 = 4.186 \text{ ms}$$

As  $t_t > t_d$ , the load on roof may be considered as a moving triangular pulse having the peak value of overpressure ( $p_{s0} + c_d q_0$ ) and time  $t_d$  is shown in Fig.2.13.



# CHAPTER 3

## NONLINEAR TRANSIENT DYNAMIC ANALYSIS

### 3.1 INTRODUCTION

Structures are subjected to time varying loads such as blast, impulse, impact or earthquake loading. Finite element based methods are available for dealing with such problems. In nonlinear transient dynamic stress analysis, it is a general practice to use a time stepping procedure. Such direct integration schemes may be broadly classified as either explicit or implicit methods.

In Explicit schemes, which are very popular, unknowns are directly solved for. The equilibrium is satisfied at each time step. However, the method is conditionally stable and very small time steps are often needed.

Implicit schemes are unconditionally stable and longer time steps can be used. A set of linear simultaneous equations is to be solved for determining the unknowns. As matrix factorisation is required, more computational effort is needed in this method.

There are three main algorithms used in nonlinear transient dynamic stress analysis. They are:

- (a) An implicit solution algorithm
- (b) An explicit solution algorithm
- (c) A combined implicit-explicit algorithm

For plane stress, plane strain and axisymmetric problems, 4, 8 and 9-noded isoparametric elements are used.

### 3.2 DYNAMIC EQUILIBRIUM EQUATION

We know that, in case of static loads(15),

$$[k]_e\{\delta\} = \{F\} + \{F\}_s + \{F\}_b$$

where

$$[k]_e = \text{Stiffness matrix} = \int_v [B]^T [D] [B] dv$$

$$\{F\}_s = \text{Surface loads} = \int_s [N]^T \{t\} ds$$

$$\{F\}_b = \text{Body forces} = \int_v [N]^T \{b\} dv$$

Due to dynamic loads, two additional forces (per unit volume) are generated in the body. They are:

(a) Inertia force -  $\rho \ddot{\delta}$

(b) Damping force -  $\mu \dot{\delta}$

where  $\dot{\delta}$  represents velocity and  $\ddot{\delta}$  represents acceleration.

$$\rho = \text{mass/unit volume}$$

$$\mu = \text{Damping coefficient for linear and viscous damping}$$

The body forces in case of dynamic loads will be,

$$\{F\}_b = \int [N]^T \{ -\rho \ddot{\delta} - \mu \dot{\delta} + b \}$$

We also know the fundamental expressions,

$$\{f\} = [N] \{\delta\}$$

$$\{\sigma\} = [D] \{\epsilon\}$$

$$\{\epsilon\} = [B] \{\delta\}$$

By the principle of virtual work, Internal workdone is equal to External workdone.

Internal workdone will be,

$$\int_v \{\delta \epsilon\}^T \{\sigma\} dv = \{\delta \delta\}^T \int_v [B]^T [D] [B] dv \{\delta\}$$

External workdone will be,

$$= \{d\delta\}^T \int_V \{-[N]^T \rho [N] \{\ddot{\delta}\} - [N]^T \mu [N] \{\dot{\delta}\} + [N]^T \{b\}\} dv$$

Equating internal workdone and external workdone and rearranging,

$$\begin{aligned} & \int_V [B]^T [D] [B] dv \{\delta\} + \int_V [N]^T \rho [N] dv \{\ddot{\delta}\} + \int_V [N]^T \mu [N] dv \{\dot{\delta}\} \\ &= \{F\} + \int_V [N]^T \{t\} ds + \int_V [N]^T \{b\} dv \\ & [K] \{\delta\} + [M] \{\ddot{\delta}\} + [C] \{\dot{\delta}\} = \{F\} + \{F\}_s + \{F\}_b \\ & [M] \{\ddot{\delta}\} + [C] \{\dot{\delta}\} + [K] \{\delta\} = \{\bar{F}\} \end{aligned} \quad (3.1)$$

where,

$$[K] = \text{Stiffness matrix} = \int_V [B]^T [D] [B] dv$$

$$[M] = \text{Consistent mass matrix} = \int_V [N]^T \rho [N] dv$$

$$[C] = \text{Damping matrix} = \int_V [N]^T \mu [N] dv$$

The above equation is known as the Dynamic equilibrium equation.

For simplicity, mass and damping matrices are assumed to be not varying with time.

### 3.3 IMPLICIT TIME SCHEMES

#### 3.3.1 Newmark's Algorithm

The predictor-corrector form of Newmark's scheme is suitable for the integration of the semi-discrete system of equations which govern nonlinear transient dynamic problems. In this algorithm, the equilibrium of equations will be at time  $(t_n + \Delta t)$ .  $a_{n+1}$ ,  $P_{n+1}$ ,  $f_{n+1}$  are the acceleration vector, internal force and applied force vector respectively.  $K_T$  and  $C_T$  are the

tangent stiffness and damping matrices respectively.  $d_n$ ,  $v_n$  and  $a_n$  are the approximations to  $d(t_n)$ ,  $\dot{d}(t_n)$  and  $\ddot{d}(t_n)$  and  $\beta$  and  $\gamma$  are parameters which control the accuracy and stability of the method. The values  $\tilde{d}_{n+1}$  and  $\tilde{v}_{n+1}$  are predictor values and  $d_{n+1}$  and  $v_{n+1}$  are corrector values. The algorithm is described in the following steps:

(a) Set iteration counter  $i = 0$ .

(b) Begin predictor phase by setting

$$\begin{aligned} d_{n+1}^{(i)} &= \tilde{d}_{n+1} = d_n + \Delta t v_n + \Delta t^2 (1-2\beta) a_n/2 \\ v_{n+1}^{(i)} &= \tilde{v}_{n+1} = v_n + \Delta t (1-\gamma) a_n \\ a_{n+1}^{(i)} &= [d_{n+1}^{(i)} - \tilde{d}_{n+1}]/(\Delta t^2\beta) = 0 \end{aligned}$$

(c) Evaluate residual forces using the equation

$$j^{(i)} = f_{n+1} - M a_{n+1}^{(i)} - p(d_{n+1}^{(i)}, v_{n+1}^{(i)})$$

(d) If required, form the effective stiffness matrix using the expression

$$K^* = M/(\Delta t^2\beta) + \gamma C_T/(\Delta t\beta) + K_T(d_{n+1}^{(i)})$$

Otherwise use a previously calculated  $k^*$ .

(e) Factorise, forward reduction and backsubstitute as required to solve

$$K^* \Delta d^{(i)} = \psi^{(i)}$$

(f) Enter corrector phase and set

$$\begin{aligned} d_{n+1}^{(i+1)} &= d_{n+1}^{(i)} + \Delta d^{(i)} \\ a_{n+1}^{(i+1)} &= \left[ d_{n+1}^{(i+1)} - \tilde{d}_{n+1} \right] / (\Delta t^2\beta) \\ v_{n+1}^{(i+1)} &= v_{n+1} + \Delta t \gamma a_{n+1}^{(i+1)} \end{aligned}$$

(g) If  $\Delta d^{(i)}$  and/or  $\psi^{(i)}$  do not satisfy the convergence conditions then set  $i = i+1$  and go to Step 3, otherwise continue.

$$(h) \text{ Set } \begin{aligned} d_{n+1} &= d_{n+1}^{(i+1)} \\ v_{n+1} &= v_{n+1}^{(i+1)} \\ a_{n+1} &= a_{n+1}^{(i+1)} \end{aligned}$$

for use in the next time step. Also set  $n = n+1$ , form  $p$  and begin next time step.

### 3.3.2 Predictor-Corrector Algorithm

This is an explicit algorithm associated with the Newmark scheme. In explicit predictor-corrector algorithm, it is assumed that the mass matrix  $M$  is diagonal and the expression

$$M a_{n+1} + p(\tilde{d}_{n+1}, \tilde{v}_{n+1}) = f_{n+1}$$

is used. The algorithm is described in the following steps:

(a) Begin predictor phase by setting

$$\begin{aligned} d_{n+1}^{(0)} &= \tilde{d}_{n+1} = d_n + \Delta t v_n + \Delta t^2 (1-2\beta)a_n/2 \\ v_{n+1}^{(0)} &= \tilde{v}_{n+1} = v_n + \Delta t (1-\gamma) a_n \\ a_{n+1}^{(0)} &= 0 \end{aligned}$$

(b) Evaluate the residual forces using the equation

$$\psi^{(0)} = f_{n+1} - p(d_{n+1}^{(0)}, v_{n+1}^{(0)})$$

(c) If required, form the effective stiffness matrix

$$K^* = M/(\Delta t^2 \beta)$$

As the Mass matrix does not change,  $k^*$  will be formed once only.

(d) Perform factorisation, forward reduction and backsubstitution as required to solve

$$K^* \Delta d^{(0)} = \psi^{(0)}$$

(e) Enter the corrector phase and set

$$d_{n+1}^{(1)} = d_{n+1}^{(0)} + \Delta d^{(0)}$$

$$a_{n+1}^{(1)} = \left[ d_{n+1}^{(1)} - \bar{d}_{n+1} \right] / (\Delta t^2 \beta)$$

$$v_{n+1}^{(1)} = v_{n+1} + \Delta t \gamma a_{n+1}^{(1)}$$

(f) Set

$$d_{n+1} = d_{n+1}^{(1)}$$

$$v_{n+1} = v_{n+1}^{(1)}$$

$$a_{n+1} = a_{n+1}^{(1)}$$

for use in the next time step. Also set  $n = n+1$ , form P and begin next time step.

### 3.4 IMPLICIT-EXPLICIT ALGORITHMS.

The computational advantages of explicit schemes are counterbalanced by the small time steps necessary. In such situations, implicit schemes permit the use of larger time steps, the size of which is governed only by accuracy considerations. Unfortunately, implicit schemes require matrix factorisations and hence need larger computer core storage and operations per time step. To overcome the above, combined implicit-explicit schemes offer a unified approach to problems of structural dynamics leading to significant computational advantages.

A combination of the previous two algorithms gives two groups of elements namely the implicit and the explicit, in the finite element mesh. In the combined algorithm, iteration within each time step is necessary in order to satisfy the equation,

$$M a_{n+1} + p^I (d_{n+1}, v_{n+1}) + p^E (\bar{d}_{n+1}, \bar{v}_{n+1}) = f_{n+1}$$

in which  $M = M^I + M^E$  and  $f_{n+1} = f_{n+1}^I + f_{n+1}^E$ .

$M^E$  is assumed to be diagonal. The implicit-explicit algorithm is described in the following steps:

(a) Set iteration counter  $i = 0$

(b) Begin predictor phase by setting

$$\mathbf{d}_{n+1}^{(i)} = \tilde{\mathbf{d}}_{n+1} = \mathbf{d}_n + \Delta t \mathbf{v}_n + \Delta t^2(1-2\beta) \mathbf{a}_n/2$$

$$\mathbf{v}_{n+1}^{(i)} = \tilde{\mathbf{v}}_{n+1} = \mathbf{v}_n + \Delta t (1-\gamma) \mathbf{a}_n$$

$$\mathbf{a}_{n+1}^{(i)} = \left[ \mathbf{d}_{n+1}^{(i)} - \tilde{\mathbf{d}}_{n+1} \right] / (\Delta t^2 \beta) = 0$$

(c) Evaluate residual forces using the equation

$$\psi^{(i)} = \mathbf{f}_{n+1} - M \mathbf{a}_{n+1}^{(i)} - \mathbf{p}^I(\mathbf{d}_{n+1}^{(i)}, \mathbf{v}_{n+1}^{(i)}) - \mathbf{p}^E(\tilde{\mathbf{d}}_{n+1}, \tilde{\mathbf{v}}_{n+1})$$

(d) If required, form the effective stiffness matrix using the expression

$$\mathbf{K}^* = M / (\Delta t^2 \beta) + \gamma \mathbf{C}_T^I / (\Delta t \beta) + \mathbf{K}_T^I(\mathbf{d}_{n+1}^{(i)})$$

Otherwise use a previously calculated  $\mathbf{K}^*$ .

(e) Perform factorisation, forward reduction and backsubstitution as required to solve,

$$\mathbf{K}^* \Delta \mathbf{d}^{(i)} = \psi^{(i)}$$

(f) Enter corrector phase by setting

$$\mathbf{d}_{n+1}^{(i+1)} = \mathbf{d}_{n+1}^{(i)} + \Delta \mathbf{d}^{(i)}$$

$$\mathbf{a}_{n+1}^{(i+1)} = \left[ \mathbf{d}_{n+1}^{(i+1)} - \tilde{\mathbf{d}}_{n+1} \right] / (\Delta t^2 \beta)$$

$$\mathbf{v}_{n+1}^{(i+1)} = \mathbf{v}_{n+1} + \Delta t \gamma \mathbf{a}_{n+1}^{(i+1)}$$

(g) If  $\Delta \mathbf{d}^{(i)}$  and/or  $\psi^{(i)}$  do not satisfy the convergence conditions, then set  $i = i+1$  and go to step 3, otherwise continue.

(h) Set  $d_{n+1}^{(i+1)} = d_{n+1}^{(i+1)}$   
 $v_{n+1}^{(i+1)} = v_{n+1}^{(i+1)}$   
 $a_{n+1}^{(i+1)} = a_{n+1}^{(i+1)}$

for use in the next time step. Also set  $n = n+1$ , form  $p$  and begin next time step.



# CHAPTER 4

## ELASTO - PLASTIC FINITE ELEMENT ANALYSIS

### 4.1 INTRODUCTION

The finite element method is now firmly accepted as one of the most powerful general techniques for the numerical solution of a variety of problems encountered in engineering. For linear analysis, at least, the technique is widely employed as a design tool. Similar acceptance for non-linear situations is dependent on two major factors. Firstly, in view of the increased numerical operations associated with non-linear problems, considerable computing power is required. With the arrival of high speed digital computers, reductions in unit computing cost will continue. Secondly, before the finite element method can be used in design, the accuracy of any proposed solution technique must be proven. The development of improved element characteristics, more efficient non-linear solution algorithms and the experience gained in their application to engineering problems have all ensured that non-linear finite element analysis can now be performed with some confidence.

Non-linearities arise in engineering situations from several sources. For example, a nonlinear material response can result from elasto-plastic material behaviour or from hyper-elastic effects of some form. Additionally nonlinear characteristics can be associated with temporal effects such as visco-elastic behaviour or dynamic transient phenomena. Each of these non-linearities may occur in a variety of structural types such as two or three dimensional solids, frames, plates or shells(8).

## **4.2 PRELIMINARY THEORY FOR TWO DIMENSIONAL ELASTO-PLASTIC APPLICATIONS**

Although there is a wide choice of element types for an elasto-plastic stress analysis, we consider three different element types of isoparametric formulation. They are:

- (a) The 4-node isoparametric quadrilateral element with linear displacement variation.
- (b) The 8-node serendipity quadrilateral element with curved sides and a quadratic variation of the displacement field within the element.
- (c) The 9-node lagrangian quadrilateral element which additionally has a central node.

The use of these higher order elements leads to particularly efficient elasto-plastic solution packages. For the plasticity applications, the classical incremental theory is employed with the full elasto plastic material response being reproduced. Consideration is limited to small deformation situations where the strains can be assumed to be infinitesimal and Lagrangian and Eulerian geometric descriptions coincide.

The computation times of elasto-plastic problems are relatively high with solution costs being typically ten times those of the corresponding linear elastic analysis. Considering the high cost of computation, it is imperative that the algorithms developed are very efficient and numerical techniques which reduce the computational requirements are employed.

## **4.3 LINEAR ELASTIC CONSTITUTIVE MATRIX FOR PLANE STRESS PLANE STRAIN AND AXISYMMETRIC CASES**

### **4.3.1 Plane Stress Problems**

Consider a typical plane stress problem. A thin plate is subjected to

loads applied in XY plane (the plane of the structure). The thickness of the plate is assumed to be small compared with the plan dimensions in the XY plane. Stresses are assumed to be constant throughout the thickness of the plate and  $\sigma_z$ ,  $\tau_{zx}$  and  $\tau_{zy}$  are ignored. The linear elastic constitutive matrix is given as

$$D = \frac{E}{(1 - \nu^2)} \begin{bmatrix} 1 & \nu & 0 \\ \nu & 1 & 0 \\ 0 & 0 & \frac{(1-\nu)}{2} \end{bmatrix}$$

#### 4.3.2 Plane Strain Problems

For plane strain problems, the thickness dimension normal to a certain plane (say the XY plane) is large compared with the typical dimensions in the XY plane and the body is subjected to loads in the XY plane only. For plane strain problems, it may be assumed that the displacements in the Z direction are negligible and that the inplane displacements u and v are independent of z. The linear elastic constitutive matrix is given as

$$D = \frac{E}{(1+\nu)(1-2\nu)} \begin{bmatrix} (1-\nu) & \nu & 0 \\ \nu & (1-\nu) & 0 \\ 0 & 0 & \frac{(1-2\nu)}{2} \end{bmatrix}$$

#### 4.3.3 Axisymmetric Problems

For a three dimensional solid which is symmetrical about its centre line axis (which coincides with the z axis) and which is subjected to loads and boundary conditions that are symmetrical about this axis, then the

behaviour is independent of the circumferential coordinate  $\theta$ . The linear elastic constitutive matrix is given as

$$D = \frac{E}{(1+\nu)(1-2\nu)} \begin{bmatrix} (1-\nu) & \nu & 0 & 0 \\ \nu & (1-\nu) & \nu & 0 \\ 0 & \nu & (1-\nu) & 0 \\ 0 & 0 & 0 & \frac{(1-2\nu)}{2} \end{bmatrix}$$

#### 4.4 ISOPARAMETRIC FINITE ELEMENT REPRESENTATION

Isoparametric elements which are extensively used in two and three dimensional problems, have the same interpolation function for the unknown functional and geometry. The shape functions are defined in natural coordinates.

For a two dimensional problem, we define the variation of unknown functional  $u$  and  $v$  as

$$\begin{aligned} u &= \sum_{i=1}^n N_i u_i \\ v &= \sum_{i=1}^n N_i v_i \end{aligned} \tag{4.1}$$

where,  $n$  represents number of nodes in the element

$N_i$  represents shape functions in  $\xi$  and  $\eta$  directions.

Further, for isoparametric elements,  $x$  and  $y$  are defined as

$$x = \sum_{i=1}^n N_i x_i \tag{4.2}$$

$$y = \sum_{i=1}^n N_i y_i$$

where  $x, y$  represent coordinates of any point within the element and  $x_i, y_i$  represent coordinates of nodal points.

#### 4.4.1 Jacobian Matrix

For two dimensional problems, we have,

$$\{\epsilon\} = \begin{Bmatrix} \epsilon_x \\ \epsilon_y \\ \gamma_{xy} \end{Bmatrix} = \begin{Bmatrix} du/dx \\ dv/dy \\ \frac{du}{dy} + \frac{dv}{dx} \end{Bmatrix}$$

From equation (4.1), we have,

$$\frac{\partial u}{\partial x} = \sum_{i=1}^n \frac{\partial N_i}{\partial x} * u_i$$

$$\frac{\partial v}{\partial y} = \sum_{i=1}^n \frac{\partial N_i}{\partial y} * v_i$$

$$\frac{\partial u}{\partial y} + \frac{\partial v}{\partial x} = \sum_{i=1}^n \frac{\partial N_i}{\partial y} u_i + \sum_{i=1}^n \frac{\partial N_i}{\partial x} v_i$$

The strain displacement matrix [B] will be,

$$[B] = \begin{bmatrix} \frac{\partial N_1}{\partial x} & 0 & \frac{\partial N_2}{\partial x} & 0 & \dots\dots\dots \\ 0 & \frac{\partial N_1}{\partial y} & 0 & \frac{\partial N_2}{\partial y} & \dots\dots\dots \\ \frac{\partial N_1}{\partial y} & \frac{\partial N_1}{\partial x} & \frac{\partial N_2}{\partial y} & \frac{\partial N_2}{\partial x} & \dots\dots\dots \end{bmatrix}$$

For isoparametric elements, the shape functions are in terms of  $\xi$  and  $\eta$  while the elements of [B] matrix contain global derivatives of shape function. Hence a transformation will be necessary.

$$\frac{\partial N_i}{\partial \xi} = \frac{\partial N_i}{\partial x} * \frac{\partial x}{\partial \xi} + \frac{\partial N_i}{\partial y} * \frac{\partial y}{\partial \xi}$$

(4.3)

$$\frac{\partial N_i}{\partial \eta} = \frac{\partial N_i}{\partial x} * \frac{\partial x}{\partial \eta} + \frac{\partial N_i}{\partial y} * \frac{\partial y}{\partial \eta}$$

In matrix form,

$$\begin{Bmatrix} \frac{\partial N_i}{\partial \xi} \\ \frac{\partial N_i}{\partial \eta} \end{Bmatrix} = \begin{bmatrix} \frac{\partial x}{\partial \xi} & \frac{\partial y}{\partial \xi} \\ \frac{\partial x}{\partial \eta} & \frac{\partial y}{\partial \eta} \end{bmatrix} \begin{Bmatrix} \frac{\partial N_i}{\partial x} \\ \frac{\partial N_i}{\partial y} \end{Bmatrix}$$

The Jacobin matrix [J] will be evaluated as

$$[J] = \begin{bmatrix} \frac{\partial x}{\partial \xi} & \frac{\partial y}{\partial \xi} \\ \frac{\partial x}{\partial \eta} & \frac{\partial y}{\partial \eta} \end{bmatrix}$$

$$[J] = \begin{bmatrix} \sum \frac{\partial N_i}{\partial \xi} x_i & \sum \frac{\partial N_i}{\partial \xi} y_i \\ \sum \frac{\partial N_i}{\partial \eta} x_i & \sum \frac{\partial N_i}{\partial \eta} y_i \end{bmatrix}$$

$$\begin{Bmatrix} \frac{\partial N_i}{\partial \xi} \\ \frac{\partial N_i}{\partial \eta} \end{Bmatrix} = [J] \begin{Bmatrix} \frac{\partial N_i}{\partial x} \\ \frac{\partial N_i}{\partial y} \end{Bmatrix} \quad (4.4)$$

Also,

$$\begin{Bmatrix} \frac{\partial N_i}{\partial x} \\ \frac{\partial N_i}{\partial y} \end{Bmatrix} = [J]^{-1} \begin{Bmatrix} \frac{\partial N_i}{\partial \xi} \\ \frac{\partial N_i}{\partial \eta} \end{Bmatrix} \quad (4.5)$$

#### 4.4.2 Stiffness Matrix of the Element

$$[K]_e = \int_v [B]^T [D] [B] dx.dy.t$$

$$[K]_e = \int_v [B]^T [D] [B] |J| d\xi d\eta.t \quad (4.6)$$

For isoparametric elements, the stiffness matrix is evaluated using numerical integration. In the equation (4.6), all the matrices can be expressed in terms of  $\xi$  and  $\eta$ . However, we cannot in general evaluate the integral exactly because of the complexity of the expressions as the determinant  $|J|$  involves polynomials in  $\xi$  and  $\eta$  which appear in the denominator. Hence the integration for computing the stiffness matrix is usually done by resorting to numerical procedures. Although there are various methods of numerical integration, Gauss Quadrature is widely adopted in finite element method. In Gauss Quadrature, both the position of sampling points and weights have been optimised. By this, we achieve a far greater level of accuracy than the accuracy achieved by other methods. In Gauss Quadrature, the integration is exact for the polynomial of order  $(2n-1)$  if  $n$  sampling points are used (3).

$$[K]_e = \int_v [B]^T [D] [B] dv = \sum_{i=1}^m \sum_{j=1}^n W_i W_j \phi(\xi_i, \eta_j)$$

## 4.5 TWO DIMENSIONAL ELASTO-PLASTIC PROBLEMS

### 4.5.1 Introduction

Most of the problems encountered in engineering can be approximated to satisfy one of three conditions of plane stress, plane strain and axisymmetric problems. The basic laws governing elasto-plastic material behaviour in two dimensional solids conforming to plane stress, plane strain or axisymmetric condition and the concepts of plastic potential and the normality condition need to be understood. The situation is complicated by the fact that different classes of materials exhibit different elasto-plastic



characteristics. The Tresca and Von Mises laws closely approximate metal plasticity behaviour while Mohr-Coulomb and Drucker-Prager criteria apply to concrete, rocks and soils.

#### **4.5.2 The Mathematical Theory of Plasticity**

The object of the mathematical theory of plasticity is to provide a theoretical description of the relationship between stress and strain for a material which exhibits an elasto-plastic response. The plastic behaviour is characterised by an irreversible straining which is not time dependent and which can only be sustained once a certain level of stress has been reached. In order to formulate a theory which models elasto-plastic material deformation three requirements have to be met. They are:

- (a) An explicit relationship between stress and strain must be formulated to describe material behaviour under elastic conditions.
- (b) A yield criterion indicating the stress level at which plastic flow commences, must be postulated.
- (c) A relationship between stress and strain must be developed for post yield behaviour when the deformation is made up of both elastic and plastic components.

#### **4.5.3 General form of the yield criteria**

The yield criterion determines the stress level at which plastic deformation begins and can be written in the general form

$$f(\sigma_{ij}) = K(k)$$

where  $f$  is some function and  $K$  a material parameter to be determined experimentally and may be a function of hardening parameter  $k$ . Any yield criterion should be independent of the orientation of the coordinate system

employed and therefore it should be a function of the three stress invariants only. Experimental observations indicate that plastic deformation of metals is essentially independent of hydrostatic pressure and hence the yield function can only be of the form

$$f(J'_2, J'_3) = K(k)$$

where  $J'_2$  and  $J'_3$  are the second and third invariants of the deviatoric stresses.

### The Tresca yield criteria

This states that yielding begins when the maximum shear stress reaches a certain value. If the principal stresses are  $\sigma_1, \sigma_2, \sigma_3$  where  $\sigma_1 \geq \sigma_2 \geq \sigma_3$ , then yielding begins when

$$\sigma_1 - \sigma_3 = Y(k)$$

where  $Y$  is a material parameter to be experimentally determined and which may be a function of the hardening parameter  $k$ . By considering all other possible maximum shearing stress values, it can be shown that this yield criterion may be represented in the  $\sigma_1\sigma_2\sigma_3$  stress space by the surface of an infinitely long regular cylinder as shown in Fig.4.1. The axis of cylinder coincides with the space diagonal, defined by points  $\sigma_1 = \sigma_2 = \sigma_3$  and since each normal section of the cylinder is identical, it is convenient to represent the yield surface geometrically by projecting it onto  $\pi$  plane,  $\sigma_1 + \sigma_2 + \sigma_3 = 0$  as shown in Fig.4.2(a). When the yield function  $f$  depends on  $J'_2$  and  $J'_3$  alone, it can be written in the form  $f(\sigma_1 - \sigma_3, \sigma_2 - \sigma_3)$  and a two dimensional plot of the surface  $f = K$  is then possible as shown in Fig.4.2(b).

## The Von Mises yield criterion

Von Mises suggested that yielding occurs when  $J'_2$  reaches a critical value.

$$(J'_2)^{1/2} = K \quad (k)$$

where  $K$  is the material parameter to be determined. The second deviatoric stress invariant,  $J'_2$  can be explicitly written as,

$$J'_2 = \frac{1}{2} \left[ \sigma_x^2 + \sigma_y^2 + \sigma_z^2 \right] + \tau_{xy}^2 + \tau_{yz}^2 + \tau_{xz}^2$$

Yield criterion may be further written as

$$\bar{\sigma} = \sqrt{3(J'_2)^{1/2}} = \sqrt{3K}$$

where  $\bar{\sigma} = \sqrt{\frac{3}{2} \{\sigma'_{ij} \sigma'_{ij}\}^{1/2}}$

and  $\bar{\sigma}$  is termed the effective stress, generalised stress or equivalent stress. The octahedral shear stress  $\tau_{oct}$ , is the shear stress on the planes of a regular octahedron, the apices of which coincide with the principal axes of stress. The value of  $\tau_{oct}$  is related to  $J'_2$  by

$$\tau_{oct} = \sqrt{(2J'_2/3)}$$

Thus yielding can be interpreted to begin when  $\tau_{oct}$  reaches a critical value. Von Mises criterion is described as in Fig.4.2. For a state of pure shear, where the Von Mises criterion gives a yield stress  $2/\sqrt{3}$  times that given by the Tresca criterion. For most metals, Von Mises law fits the experimental data more closely than Tresca's law but the Tresca criterion is simpler to use in theoretical applications.

### The Mohr-Coulomb yield criterion

This is a generalisation of the coulomb friction failure law defined by

$$\tau = c - \sigma_n \tan\phi$$

where  $\tau$  is the shearing stress,  $\sigma_n$  is the normal stress with tensile stress being positive,  $c$  is the cohesion and  $\phi$  is the angle of internal friction. Figure 4.3 represents the Coulomb's law as a straight line tangent to the largest principal stress circle.

From Fig.4.3 and for  $\sigma_1 \geq \sigma_2 \geq \sigma_3$ , the Coulomb law can be written as

$$(\sigma_1 - \sigma_3) = 2c \cos\phi - (\sigma_1 + \sigma_3) \sin\phi$$

In the principal stress space, this gives a conical yield surface whose normal section at any point is an irregular hexagon as shown in Fig.4.4. The conical nature of the yield surface is a consequence of the fact that a hydrostatic stress does influence yielding. This criterion is applicable to concrete, rocks and soil problems.

### The Drucker-Prager yield criterion

An approximation to the Mohr-Coulomb law was presented by Drucker and Prager as a modification of the Von Mises yield criterion. The influence of a hydrostatic stress component on yielding was introduced by inclusion of an additional term in the Von Mises expression to give

$$aJ_1 + (J_2')^{1/2} = k'$$

The yield surface has the form of a circular cone. This yield criterion is described as in Fig.4.4.

#### 4.5.4 Work or Strain Hardening

After initial yielding, the stress level at which further plastic deformation occurs may be dependent on the current degree of plastic straining. Such a phenomenon is termed work hardening or strain hardening. Thus the yield surface will vary at each stage of the plastic deformation, with the subsequent yield surfaces being dependent on the plastic strains. A perfectly plastic material is shown in Fig.4.5(a), where the yield stress level does not depend in any way on the degree of plastification. If the subsequent yield surfaces are a uniform expansion of the origin yield curve, without translation, as shown in Fig.4.5(b), the strain hardening model is said to be isotropic. If the subsequent yield surfaces preserve their shape and orientation but translate in the stress space as a rigid body, as shown in Fig. 4.5(c), Kinematic hardening is said to take place.

For some materials, notably soils, the yield surface may not strain harden but strain soften instead, so that the yield stress level at a point decreases with increasing plastic deformation. Therefore, for an isotropic model, the original yield curve contracts progressively without translation. Consequently yielding implies local failure and the yield surface becomes a failure criterion.

The progressive development of the yield surface can be defined by relating the yield stress  $K$  to the plastic deformation by means of the hardening parameter  $k$ .  $k$  can be related to a measure of the total plastic deformation termed the effective, generalised or equivalent plastic strain

which is defined incrementally as

$$d\bar{\epsilon}_p = \sqrt{\left(\frac{2}{3}\right) \left\{ \left(d\epsilon_{ij}\right)_p \left(d\epsilon_{ij}\right)_p \right\}^{1/2}}$$

For situations where the assumption that yielding is independent of any hydrostatic stress is valid,  $(d\epsilon_{ii})_p = 0$  and hence  $(d\epsilon'_{ij})_p = (d\epsilon_{ij})_p$ .

$$d\bar{\epsilon}_p = \sqrt{\left(\frac{2}{3}\right) \left\{ \left(d\epsilon'_{ij}\right)_p \left(d\epsilon'_{ij}\right)_p \right\}^{1/2}}$$

Then the hardening parameter,  $k$ , is assumed to be defined as

$k = \bar{\epsilon}_p$  where  $\bar{\epsilon}_p$  is the result of integration  $d\bar{\epsilon}_p$  over the strain path. This behaviour is termed strain hardening.

#### 4.5.5 Elasto-plastic Stress-Strain Relation

After initial yielding, the material behaviour will be partly elastic and partly plastic. During any increment of stress, the changes of strain are assumed to be divisible into elastic and plastic components, so that

$$d\epsilon_{ij} = (d\epsilon_{ij})_e + (d\epsilon_{ij})_p$$

Decomposing the stress terms into their deviatoric and hydrostatic components

$$(d\epsilon_{ij})_e = \frac{d\sigma'_{ij}}{2\mu} + \frac{(1-2\nu)}{E} \delta_{ij} d\sigma_{kk}$$

where  $E$  and  $\nu$  are respectively the elastic modulus and poisson's ratio of the material.

In order to derive the relationship between the plastic strain component and the stress increment, a further assumption on the material behaviour must be made. It is assumed that the plastic strain increment is

proportional to the stress gradient of a quantity termed the plastic potential  $Q$ , so that

$$(d\varepsilon_{ij})_p = d\lambda \frac{\partial Q}{\partial \sigma_{ij}}$$

where  $d\lambda$  is a proportionality constant termed the plastic multiplier. The above equation is termed the flow rule since it governs the plastic flow after yielding. The potential  $Q$  must be a function of  $J'_2$  and  $J'_3$ . However the relation  $f \equiv Q$  is valid since it has been postulated that both are functions of  $J'_2$  and  $J'_3$  and such an assumption gives rise to an associated theory of plasticity.

$(d\varepsilon_{ij})_p = d\lambda \frac{\partial f}{\partial \sigma_{ij}}$  and is termed the normality condition since  $\frac{\partial f}{\partial \sigma_{ij}}$  is a vector directed normal to the yield surface at the stress point under consideration. Experimental observations indicate that the normality condition is an acceptable assumption for metals but the question of normality in rocks and soils is debatable. The complete incremental relationship between the stress and strain for elasto-plastic deformation is found to be

$$(d\varepsilon_{ij})_p = \frac{\partial \sigma'_{ij}}{2\mu} + \frac{(1-2\nu)}{E} \delta_{ij} d\sigma_{kk} + d\lambda \frac{\partial f}{\partial \sigma_{ij}}$$

#### 4.5.6 The Yield Criteria For Numerical Computation

For numerical computations, it is convenient to rewrite the yield function in terms of alternate stress invariants. The main advantage of this formulation is that it permits the computer coding of the yield function and the flow rule in a general form and necessitates only the specification of three constants for any individual criterion.

the cubic equation

$$S'^3 - J'_2 S' - J'_3 = 0 \quad (4.7)$$

which is similar to the trigonometric identity

$$\sin^3 \theta - \frac{3}{4} \sin \theta + \frac{1}{4} \sin 3\theta = 0 \quad (4.8)$$

Substituting  $S = r(\sin \theta)$  in equation (4.7), we have

$$\sin^3 \theta - \frac{J'_2}{r^2} \sin \theta - \frac{J'_3}{r^3} = 0 \quad (4.9)$$

Comparing (4.8) and (4.9) gives

$$r = \frac{2}{\sqrt{3}} (J'_2)^{1/2} \quad (4.10)$$

$$\sin 3\theta = \frac{-4J'_3}{r^3} = -\frac{3\sqrt{3}}{2} \cdot \frac{J'_3}{(J'_2)^{3/2}} \quad (4.11)$$

By noting the cyclic nature of  $\sin(3\theta + 2n\pi)$ , there are only three possible values of  $\sin \theta$  which define the three principal stresses. The deviatoric principal stresses are given by  $t = r(\sin \theta)$  on substitution of the three values of  $\sin \theta$  in turn. The total principal stresses are

$$\begin{Bmatrix} \sigma_1 \\ \sigma_2 \\ \sigma_3 \end{Bmatrix} = \frac{2(J'_2)^{1/2}}{\sqrt{3}} \begin{Bmatrix} \sin \left( \theta + \frac{2\pi}{3} \right) \\ \sin \theta \\ \sin \left( \theta + \frac{2\pi}{3} \right) \end{Bmatrix} + \frac{J_1}{3} \begin{Bmatrix} 1 \\ 1 \\ 1 \end{Bmatrix} \quad (4.12)$$

with  $\sigma_1 > \sigma_2 > \sigma_3$  and  $-\frac{\pi}{6} \leq \theta \leq \frac{\pi}{6}$ . The four yield criteria can be rewritten in terms of  $J_1$ ,  $J'_2$  and  $\theta$ .



### 4.5.7 The Yield Criteria

#### The Tresca yield criterion

We know that,

$$\sigma_1 - \sigma_3 = Y(k)$$

Substituting for  $\sigma_1$  and  $\sigma_3$  from (4.12),

$$\frac{2}{\sqrt{3}} (J'_2)^{1/2} \left[ \sin \left( \theta + \frac{2\pi}{3} \right) - \sin \left( \theta + \frac{4\pi}{3} \right) \right] = Y(k)$$

on simplification

$$2 (J'_2)^{1/2} \cos\theta = Y(k) = \sqrt{3K(k)} = \sigma_y(k)$$

#### The Von Mises yield criterion

There is no change in this case since this yield function depends on  $J'_2$  only.

$$(J'_2)^{1/2} = K(k)$$

$$\sqrt{3(J'_2)^{1/2}} = \sigma_y(k)$$

#### The Mohr-Coulomb Yield Criterion

We know that,

$$(\sigma_1 - \sigma_3) = 2c \cos\phi - (\sigma_1 + \sigma_3) \sin\phi$$

Substituting the values of  $\sigma_1$  and  $\sigma_3$  from (4.12),

$$\frac{1}{3} J_1 \sin\phi + (J'_2)^{1/2} \left[ \cos\theta - \frac{1}{\sqrt{3}} \sin\theta \sin\phi \right] = c \cos\phi$$

## The Drucker-Prager yield criterion

There is no change for this criterion

$$a J_1 + (J_2')^{1/2} = k'$$

### 4.5.8 The flow vector for numerical computation

The flow vector  $a$  can be written as

$$a^T = \frac{\partial F}{\partial \sigma} = \frac{\partial F}{\partial J_1} \frac{\partial J_1}{\partial \sigma} + \frac{\partial F}{\partial (J_2')^{1/2}} \cdot \frac{\partial (J_2')^{1/2}}{\partial \sigma} + \frac{\partial F}{\partial \theta} \cdot \frac{\partial \theta}{\partial \sigma}$$

The above can be written in the form

$$a = c_1 a_1 + c_2 a_2 + c_3 a_3$$

where

$$C_1 = \frac{\partial F}{\partial J_1}$$

$$C_2 = \left[ \frac{\partial F}{\partial (J_2')^{1/2}} - \frac{\tan 3\theta}{(J_2')^{1/2}} \frac{\partial F}{\partial \theta} \right]$$

$$C_3 = \frac{-\sqrt{3}}{2 \cos 3\theta} \cdot \frac{1}{(J_2')^{3/2}} \cdot \frac{\partial F}{\partial \theta}$$

Only the constants  $C_1$ ,  $C_2$ ,  $C_3$  are then necessary to define the yield surface. Thus a simplicity of Programming is achieved as only these three constants have to be varied between one yield surface and another.

In two dimensional problems,

$$a^T = \left\{ \frac{\partial F}{\partial \sigma_x}, \frac{\partial F}{\partial \sigma_y}, \frac{\partial F}{\partial \tau_{xy}}, \frac{\partial F}{\partial \sigma_z} \right\}$$

For the case of axisymmetric problems,  $x$ ,  $y$  and  $z$  are replaced by  $r$ ,  $z$  and  $\theta$ .

$$a_1^T = \{1, 1, 0, 1\}$$

$$a_2^T = \frac{1}{2(J_2')^{1/2}} \left\{ \sigma'_x, \sigma'_y, 2\tau_{xy}, \sigma'_z \right\}$$

$$a_3^T = \left\{ \left[ \sigma'_y \sigma'_z + \frac{J_2'}{3} \right], \left[ \sigma'_x \sigma'_z + \frac{J_2'}{3} \right], -2 \sigma'_z \tau_{xy}, \left[ \sigma'_x \sigma'_y - \tau_{xy}^2 + \frac{J_2'}{3} \right] \right\}$$

$$\text{where } J_2' = \frac{1}{2} \left( \sigma_x'^2 + \sigma_y'^2 + \sigma_z'^2 \right) + \tau_{xy}^2$$

$$J_3' = \sigma'_z \left( \sigma_z'^2 - J_2' \right)$$

For the elasto-plastic matrix  $D_{ep}$ , we require  $d_D$ .

The elasto-plastic constitutive matrix  $D_{ep}$ ,

$$D_{ep} = D - \frac{d_D d_D^T}{A + d_D^T a} \text{ and } d_D = D a$$

For plane strain and axisymmetric cases,

$$d_D = \begin{Bmatrix} d_1 \\ d_2 \\ d_3 \\ d_4 \end{Bmatrix} = \begin{Bmatrix} \frac{E}{1+\nu} a_1 + M_1 \\ \frac{E}{1+\nu} a_2 + M_1 \\ G a_3 \\ \frac{E}{1+\nu} a_4 + M_1 \end{Bmatrix}$$

$$M_1 = \frac{E\nu (a_1 + a_2 + a_4)}{(1+\nu)(1-2\nu)}$$

where  $a_1, a_2, a_3$  and  $a_4$  are the components of  $a$ .

For plane stress cases,

$$d_D = \left\{ \begin{array}{l} \frac{E}{1+\nu} a_1 + M_2 \\ \frac{E}{1+\nu} a_2 + M_2 \\ G a_3 \\ \frac{E}{1+\nu} a_4 + M_2 \end{array} \right\} \text{ and } M_2 = \frac{E\nu (a_1 + a_2)}{1-\nu^2}$$

#### 4.5.9 Singular Points on the Yield Surface

For many yield surfaces, the flow vector  $a$  is not uniquely defined for certain stress combinations. At the corners of the Tresca and Mohr-Coulomb criteria located by  $\theta = \pm 30$ , the direction of plastic straining is indeterminate.

For the Tresca law,

$$\sqrt{3} (J_2')^{1/2} = Y(k) = \sqrt{3} K(k) \text{ and}$$

$$C_1 = 0, C_2 = \sqrt{3}, C_3 = 0 \text{ for } \theta = \pm 30^\circ$$

For the Mohr-Coulomb criterion,

$$\frac{1}{3} J_1 \sin\phi + (J_2')^{1/2} \cdot \frac{1}{2} \left[ \sqrt{3} - \frac{\sin\phi}{\sqrt{3}} \right] - c \cos\phi = 0 \quad \text{for } \theta = + 30^\circ$$

$$\frac{1}{3} J_1 \sin\phi + (J_2')^{1/2} \cdot \frac{1}{2} \left[ \sqrt{3} + \frac{\sin\phi}{\sqrt{3}} \right] - c \cos\phi = 0 \quad \text{for } \theta = - 30^\circ$$

$$C_1 = \frac{1}{3} \sin\phi, C_2 = \frac{1}{2} \left( \sqrt{3} - \frac{\sin\phi}{\sqrt{3}} \right), C_3 = 0 \quad \text{for } \theta = +30^\circ$$

$$C_1 = \frac{1}{3} \sin\phi, C_2 = \frac{1}{2} \left( \sqrt{3} + \frac{\sin\phi}{\sqrt{3}} \right), C_3 = 0 \quad \text{for } \theta = -30^\circ$$

# CHAPTER 5

## CASE STUDIES

### 5.1 INTRODUCTION

Bunkers are primarily exposed to surface bursts. However, the possibility of bunkers being subjected to air burst loads cannot be ruled out. The effect of blast is more critical in case of above ground and semi-buried bunkers than in case of underground bunkers. Keeping in mind these aspects, for the dissertation work, three separate cases have been considered. Each of these have been analysed for various intensities of blast loads and for different distances. IS Code recommended blast loads have been made use of in the analysis.

### 5.2 FEATURES OF COMPUTER PROGRAM

The computer program used is based on the Implicit-Explicit time integration scheme for two dimensional plane stress, plane strain and axisymmetric nonlinear dynamic transient problems(8).

Four, Eight and Nine noded isoparametric elements are used to model geometric nonlinear behaviour. The program has several options like small or large deformation elastic and small deformation elasto-plastic analysis. The analysis may be carried out using an explicit, implicit or a combined explicit-implicit algorithm. Further, four types of elasto-plastic material models can be considered. They are Tresca, Von Mises, Mohr-Coulomb and Drucker-Prager.

The input data, in addition to the features mentioned earlier, includes nodal coordinates, element connectivity data, material parameters etc.. The input data also includes the node numbers at which displacement history and stress history are desired. It also includes point load, Gravity load, Pressure load and Temperature load indicators.

A post-processor subroutine specifically for blast loads recommended by IS Code has been incorporated. The post-processor aids in plotting displacement versus time graphs for the chosen nodes in both elastic and elasto-plastic analysis. The flow chart of the computer program is as shown in Fig.5.18.

### **5.3 TYPES OF BUNKERS CONSIDERED FOR ANALYSIS**

The three types of bunkers considered for analysis are:

- (a) An above ground bunker
- (b) A bunker with soil cover
- (c) A semi-buried bunker

### **5.4 THE PROBLEM DEFINITION**

#### **5.4.1 An Above Ground Bunker**

In this, a bunker of 3.0m x 2.6m is considered for analysis. The bunker has been discretized into 78 elements and 286 nodes. The thickness of walls, roof and floor slabs have all been assumed to be 30 cms. This is as shown in Fig.5.1.

#### **5.4.2 A Bunker with Soil Cover**

A bunker of same dimensions is considered for analysis. The bunker has a 60 cm soil cover all round except below the floor. The bunker has been discretized into 162 elements and 566 nodes. Of the 162 elements, 102 elements are of the bunker and the balance 60 are of soil. This is as shown in Fig.5.2.

#### **5.4.3 A Semi-Buried Bunker**

A bunker of same dimensions as considered in the previous two cases, has been analysed. The bunker is buried 1.7m deep into the soil. The bunker

has been discretized into 274 elements and 916 nodes, of which 78 are the elements of the bunker and the remaining 196 elements are of the surrounding soil. This is as shown in Fig.5.3.

## **5.5 THE BLAST LOADS ON THE BUNKERS**

A detailed description blast loads has been done in Chapter 2. The bunkers have been analysed for IS Code recommended blast loads. Blast loads of 100 kgs at 20 m, 30 kgs at 10 m and 10 kgs at 5 m have been considered for analysis.

## **5.6 RESULTS AND DISCUSSIONS**

The results and discussions of the analysis have been described under five important headings. They are:

- (a) The Geometry of Problem
- (b) Boundary Conditions
- (c) Loading Conditions
- (d) Material Parameters
- (e) Discussions

### **5.6.1 The Geometry of Problem**

It has been described under problem definition in 5.4.

### **5.6.2 Boundary Conditions**

In all the three types of bunkers, the base has been assumed to be fixed. However, from practical considerations, it can be mentioned that absolute fixity is difficult to achieve.

### **5.6.3 Loading Conditions**

The blast loads calculated as in 2.5.1, 2.5.2 and 2.5.3 have been applied on all the three types of bunkers, both on front face and roof.



#### 5.6.4 Material Parameters

The same values of material parameters have been used in all the three types of bunkers to facilitate comparative study. The material parameters of concrete and soil are as in Table 5.1.

#### 5.6.5 Discussions

In the analysis of bunkers, the self weight of the bunkers has not been considered as there was no provision for self weight to be added in the input file of the computer program. Because of the self weight, the bunkers will have been stressed to a certain level, before blast loads are applied. As a result, the levels of stress indicated by the analysis are likely to be lower than the actual stresses.

A comparison of the blast pressures generated by the three explosive weights at specified distances, indicate that blast pressure corresponding to 10 kg at 5 m produces the maximum blast pressure.

The horizontal and vertical displacements of the critical nodes of an above ground bunker for blast loads corresponding to 100 kg at 20 m ,30 kg at 10 m and 10 kg at 5 m are as shown in Fig.5.4 to Fig.5.6.

The horizontal and vertical displacements of the critical nodes of an above ground bunker with soil cover for blast loads corresponding to 100 kg at 20 m,30 kg at 10 m and 10 kg at 5 m are as shown in Fig.5.7 to Fig.5.9.

The horizontal and vertical displacements of the critical nodes of a semi-buried bunker for blast loads corresponding to 100 kg at 20 m, 30 kg at 10 m and 10 kg at 5 m are as shown in Fig.5.10 to Fig.5.12.

The deflected profile of the three bunkers under 10 kg at 5 m are as shown in Fig.5.13 to Fig.5.15.

The yielded profile of the above ground bunker and the above ground bunker with soil cover are as shown in Fig.5.16 and Fig.5.17.

The above ground bunker with soil cover has exhibited lower frequency and higher time period of vibration as compared to the above ground bunker. 60 cm of overlaying soil, although has negligible stiffness compared to concrete, increases the overall mass of the system considerably. This has resulted in higher time periods in case of above ground bunker with soil cover.

In case of above ground bunker with soil cover, the area exposed to blast pressure on both front face and roof, are greater. As a result, it exhibits larger displacements than that of an above ground bunker.

From the deflected profile of semi-buried bunker in Fig.5.15, it is clear that the semi-buried bunker has undergone rigid body translation and rotation without yielding.

Consider the above ground bunker and the above ground bunker with soil cover for checking of horizontal elastic displacements at the respective critical nodes. Assuming hinges at end nodes of the face for simplicity.

Reaction at the critical node for above ground bunker

$$= WL^2/6 = 1 * 3^2/6 = 1.5 \text{ kg}$$

Reaction at the critical node for above ground bunker with soil cover

$$= WL^2/6 = 1*(3.6)^2/6 = 2.16 \text{ kg}$$

$$\text{Ratio} = 2.16/1.5 = 1.44$$

The ratio as obtained from the graphs plotted =  $42/28 = 1.54$

The ratios are comparable with an accepted error of less than 10% indicating that the results from analysis agree well with the theoretical assessment of the ratios.

From Fig.5.16 and Fig.5.17, it clear that widespread yielding has occurred in above ground bunker and above ground bunker with soil cover.

# CHAPTER 6

## CONCLUSIONS

From the two dimensional analysis of bunkers subjected to blast loads, following conclusions have been drawn:

1. IS:4991-1968 has recommended blast load pressures corresponding to 100 kg explosive at 20 m distance, as the design blast load pressure for important civilian buildings. For military applications, explosive weights of 30 kg and 10 kg corresponding approximately to Artillery shells and Mortar shells, at distances of 10 m and 5 m provide a far more realistic design blast load pressures than the recommendations of IS Code.
2. Semi-buried bunkers have undergone rigid body rotation and translation without yielding. The above ground bunker and the above ground bunker with soil cover have both yielded under 10 kg explosive at 5 m distance.
3. In case of above ground bunker and above ground bunker with soil cover, widespread yielding has been observed indicating that merely an elastic analysis may not suffice. Therefore, elasto-plastic analysis is recommended for structures subjected to blast loads.
4. In above ground bunker with soil cover, the displacement at the critical nodes have been counter-intuitive. We expect the above ground bunker with soil cover to exhibit lesser displacements compared to the above ground bunker. But, it actually has a larger area exposed to the blast pressure because of which, the above ground bunker with soil cover exhibits larger displacements.
5. In semi-buried bunkers, high residual displacements in elasto-plastic analysis are due to the yielding of soil mass only. Here, the concrete has not yielded and has remained in the elastic zone.

6. As there is no yielding of concrete in semi-buried bunkers, it is recommended that thinner sections may also be used in semi-buried bunker constructions.
7. Semi-buried bunkers offer far better protection against blast loads than above ground bunkers. Therefore, Semi-buried bunkers are recommended for use as strategic structures.

248101



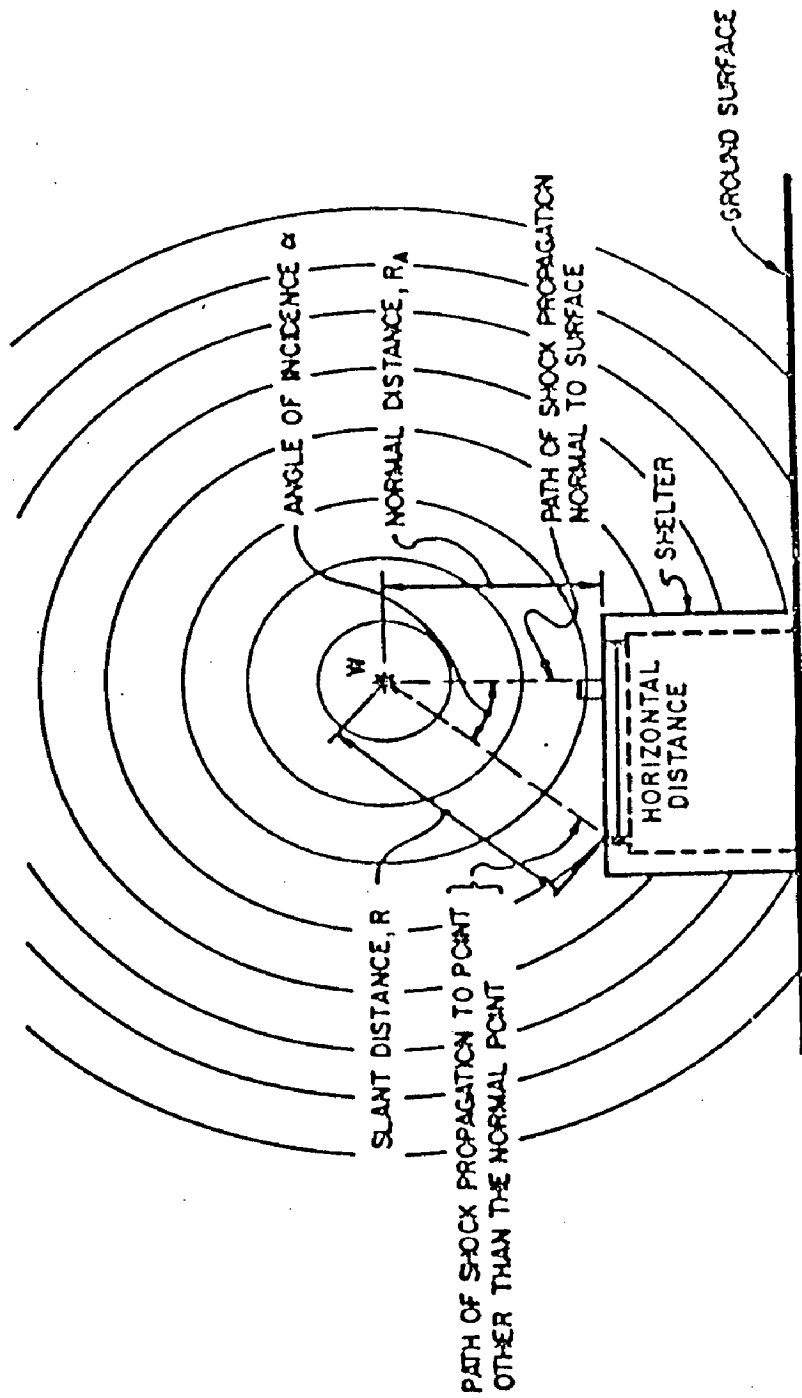
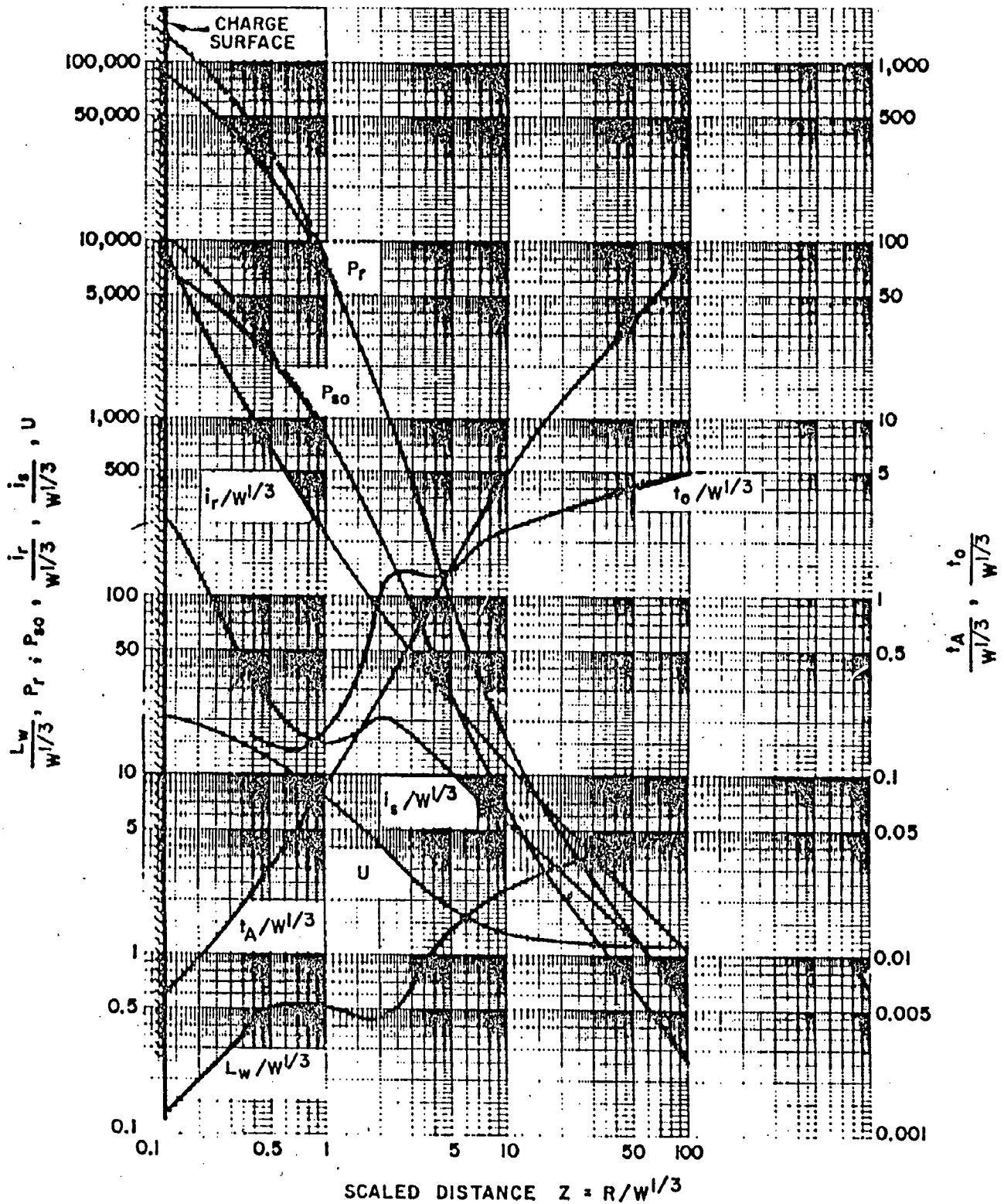


Fig. 2.1 Free-air Burst Environment



- $P_{s0}$  = PEAK POSITIVE INCIDENT PRESSURE, psi
- $P_r$  = PEAK POSITIVE NORMAL REFLECTED PRESSURE, psi
- $i_s/W^{1/3}$  = SCALED UNIT POSITIVE INCIDENT IMPULSE, psi-ms/lb<sup>1/3</sup>
- $i_r/W^{1/3}$  = SCALED UNIT POSITIVE NORMAL REFLECTED IMPULSE, psi-ms/lb<sup>1/3</sup>
- $t_A/W^{1/3}$  = SCALED TIME OF ARRIVAL OF BLAST WAVE, ms/lb<sup>1/3</sup>
- $t_0/W^{1/3}$  = SCALED POSITIVE DURATION OF POSITIVE PHASE, ms/lb<sup>1/3</sup>
- $U$  = SHOCK FRONT VELOCITY, ft/ms
- $W$  = CHARGE WEIGHT, lbs
- $L_w/W^{1/3}$  = SCALED WAVE LENGTH OF POSITIVE PHASE, ft/lb<sup>1/3</sup>

Fig. 2.2 Positive phase shock wave parameters for a spherical TNT explosion in free air at sea level

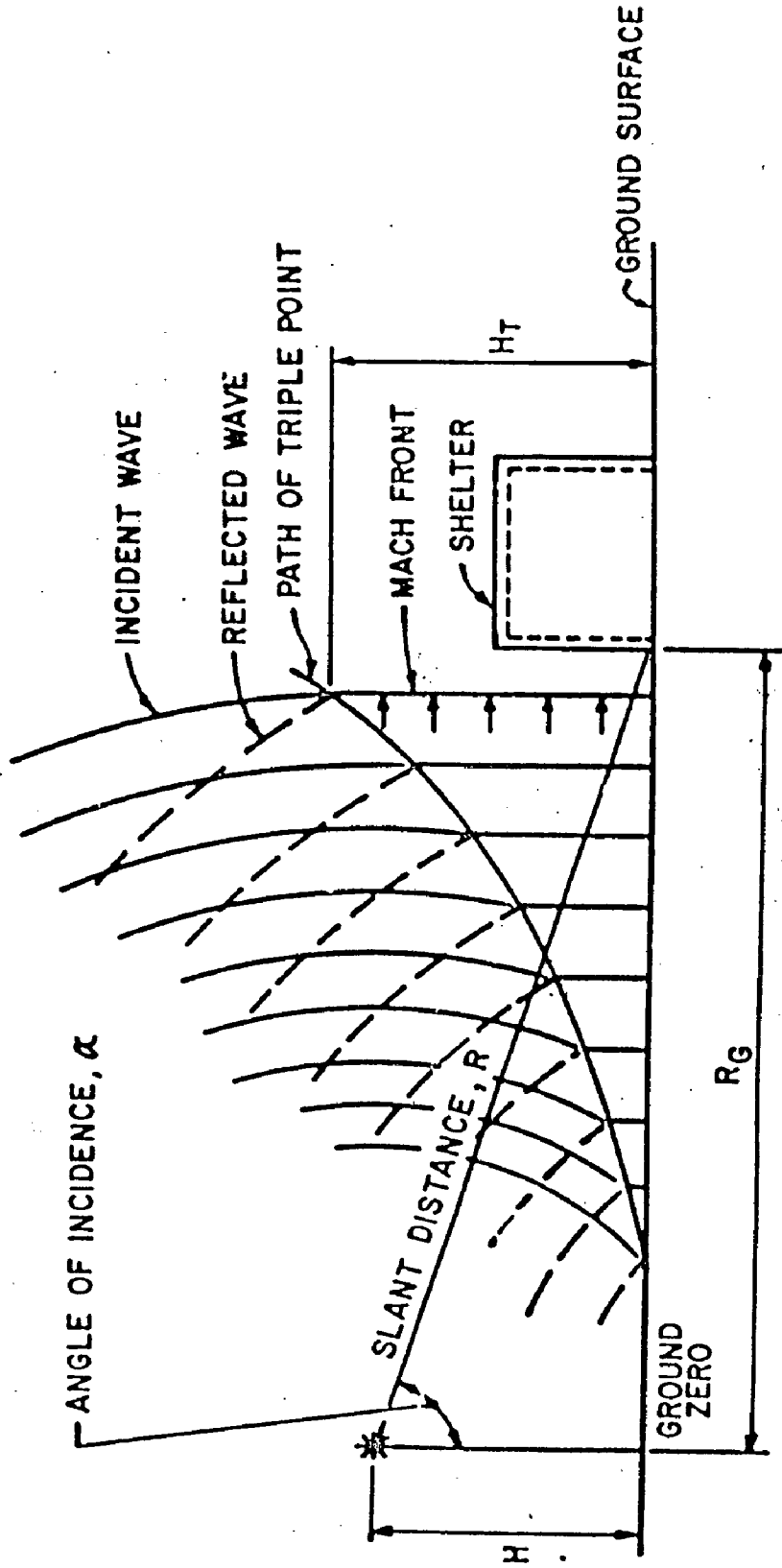


Fig. 2.3 Air Burst Blast Environment

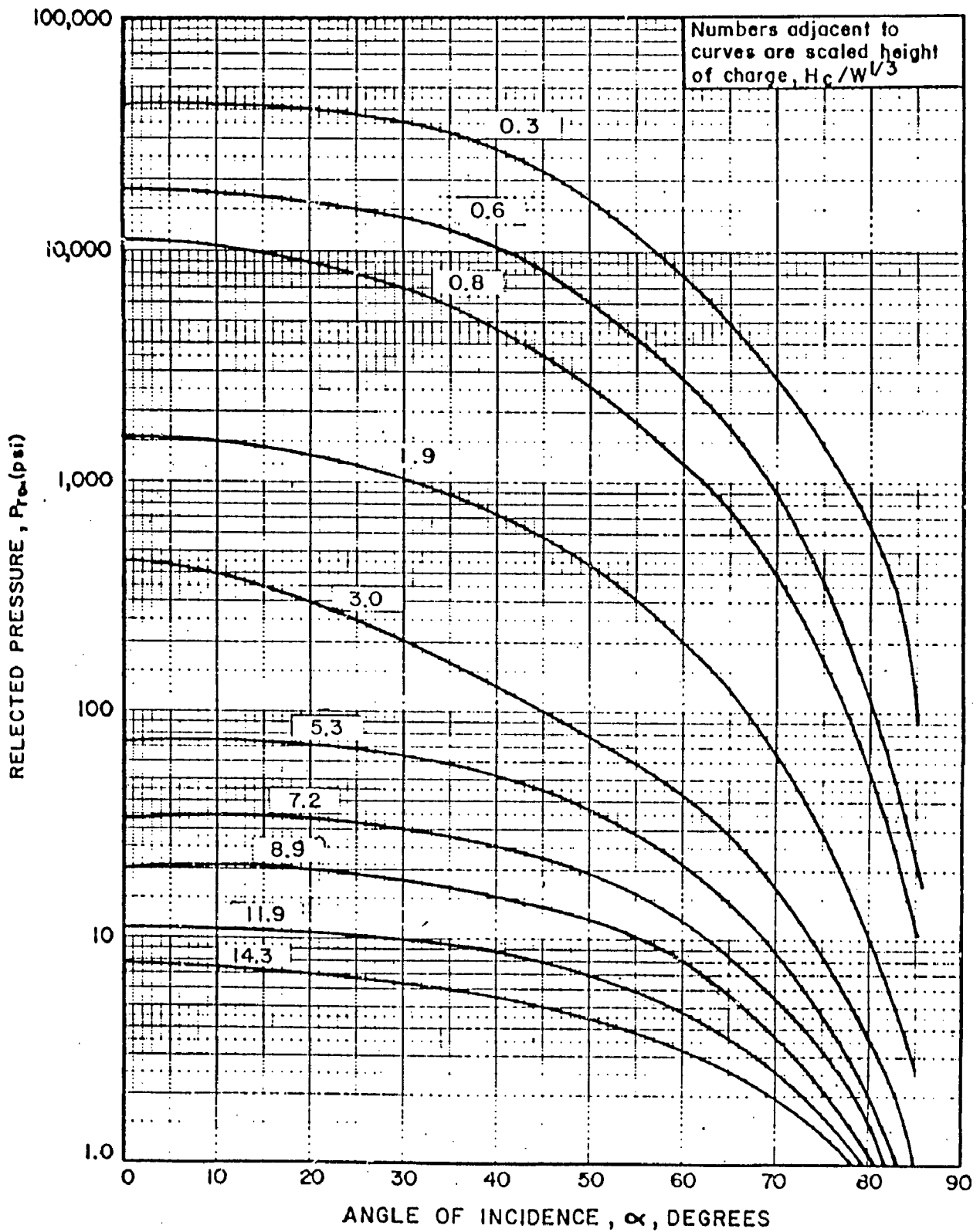


Fig. 2.4 Variation of reflected pressure as a function of angle of incidence



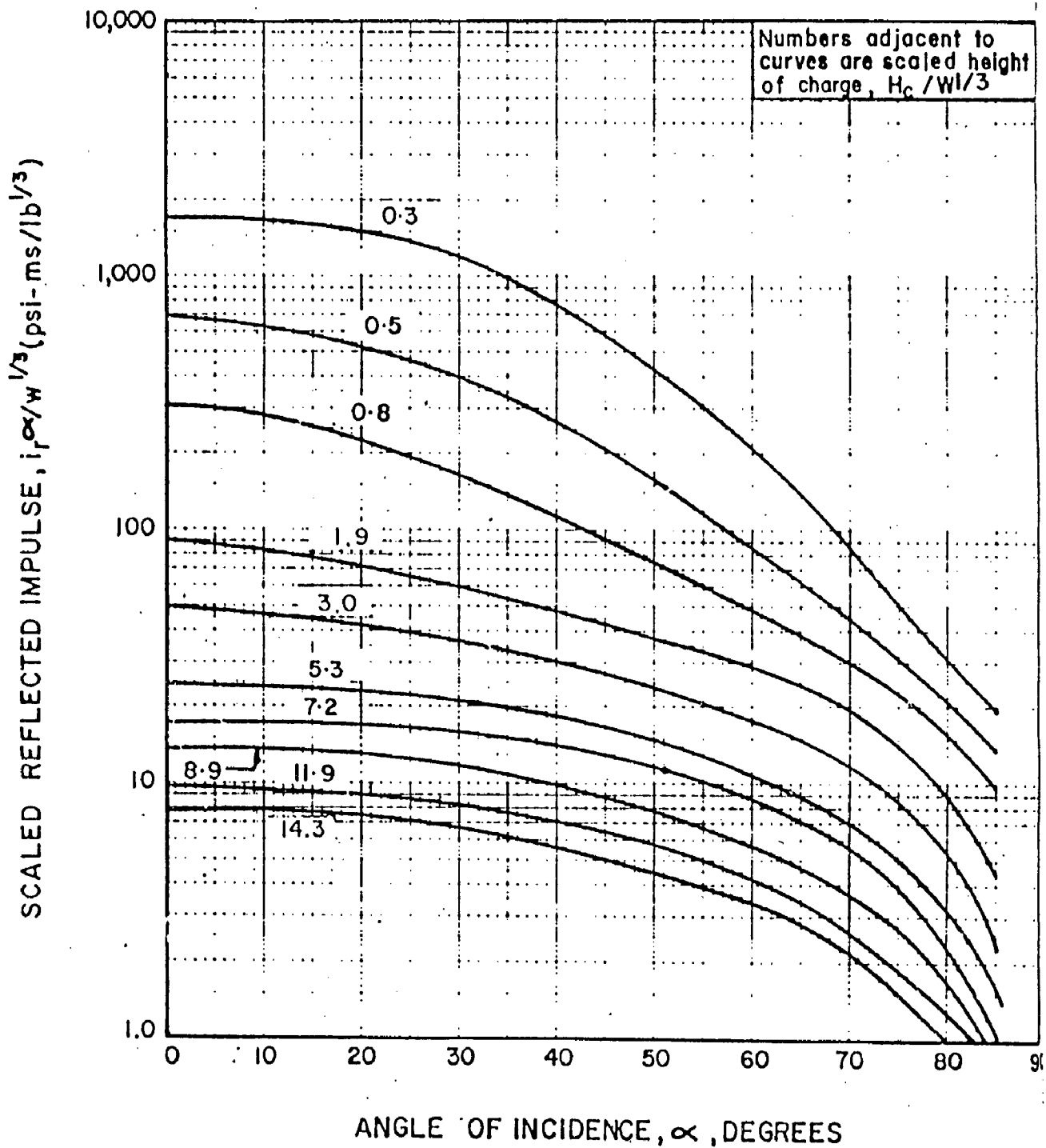


Fig. 2.5 Variation of scaled reflected impulse as a function of angle of incidence

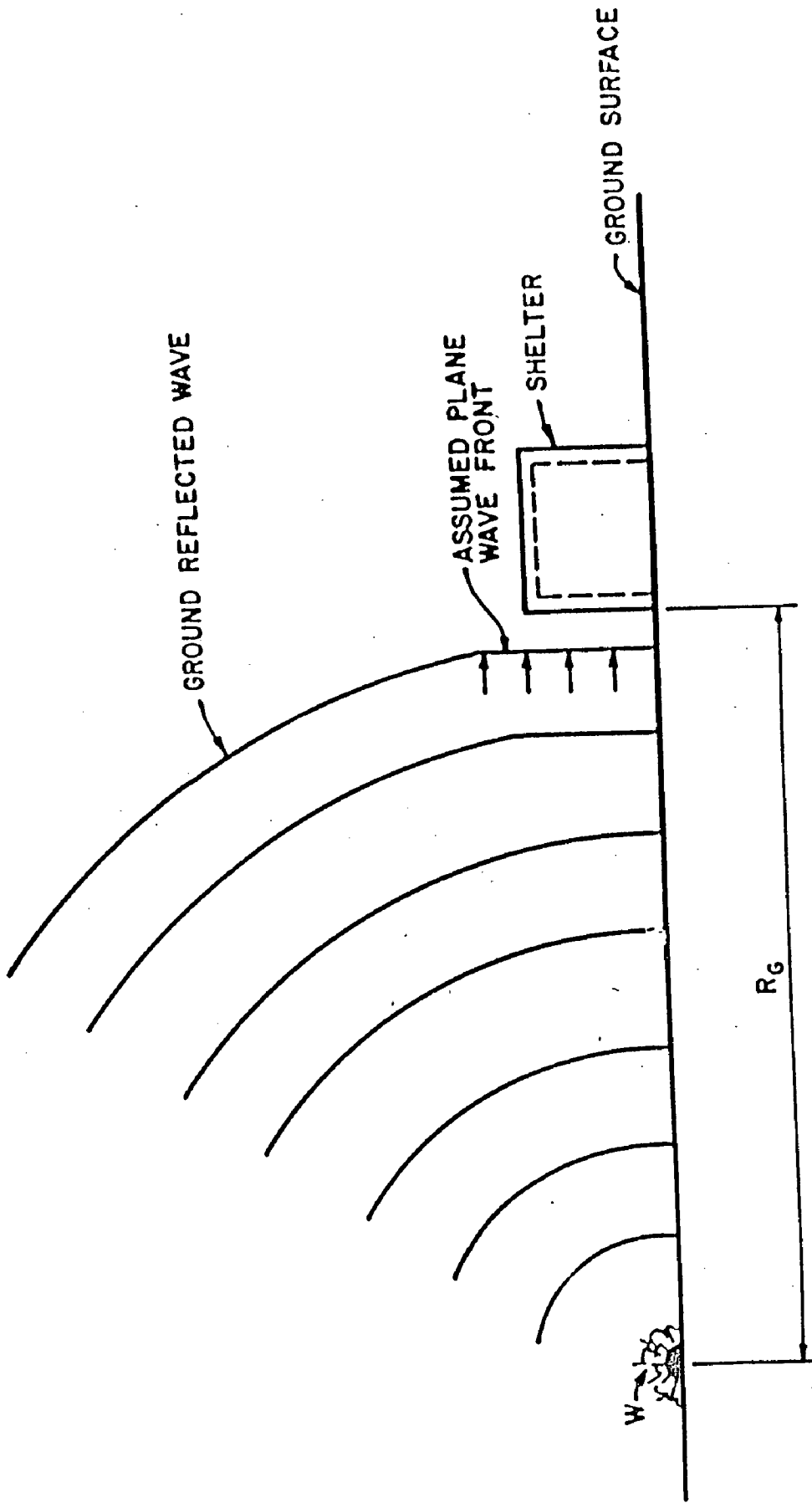
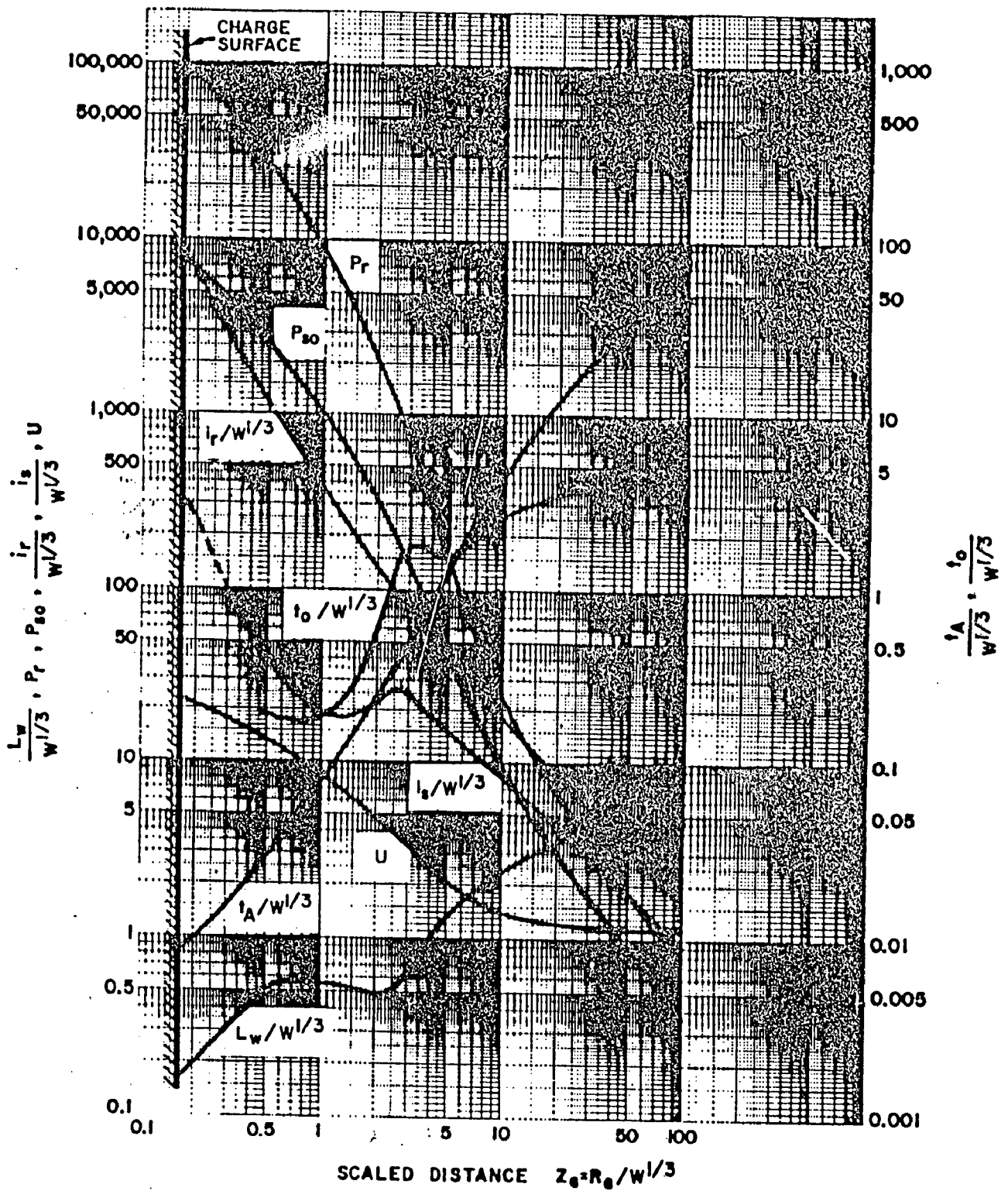


Fig. 2.6 Surface burst blast environment



- $P_{s0}$  = PEAK POSITIVE INCIDENT PRESSURE, psi
- $P_r$  = PEAK POSITIVE NORMAL REFLECTED PRESSURE, psi
- $i_s / W^{1/3}$  = SCALED UNIT POSITIVE INCIDENT IMPULSE, psi-ms/lb<sup>1/3</sup>
- $i_r / W^{1/3}$  = SCALED UNIT POSITIVE NORMAL REFLECTED IMPULSE, psi-ms/lb<sup>1/3</sup>
- $t_A / W^{1/3}$  = SCALED TIME OF ARRIVAL OF BLAST WAVE, ms/lb<sup>1/3</sup>
- $t_0 / W^{1/3}$  = SCALED POSITIVE DURATION OF POSITIVE PHASE, ms/lb<sup>1/3</sup>
- $U$  = SHOCK FRONT VELOCITY, ft/ms
- $W$  = CHARGE WEIGHT, lbs
- $L_w / W^{1/3}$  = SCALED WAVE LENGTH OF POSITIVE PHASE, ft/lb<sup>1/3</sup>

Fig. 2.7 Positive phase shock wave parameters for a hemispherical TNT explosion on the surface at sea level

# PRESSURE TIME CURVES

## CASE A : 100 KG EXPLOSIVE AT 20 M DISTANCE

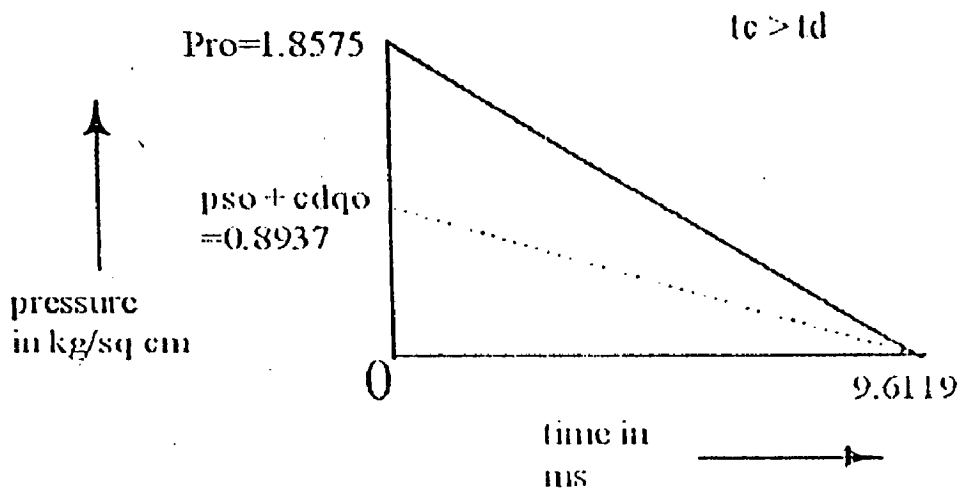


FIG 2.8 FRONT FACE LOADING

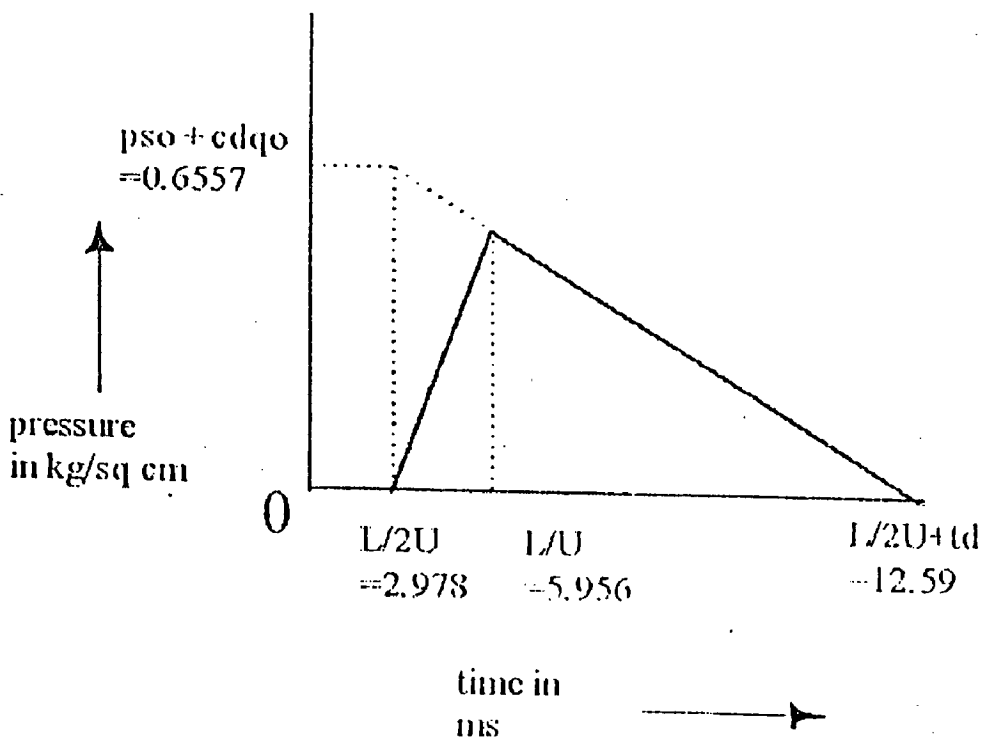


FIG 2.9 ROOF LOADING

# CASE B : 30 KG EXPLOSIVE AT 10 M DISTANCE

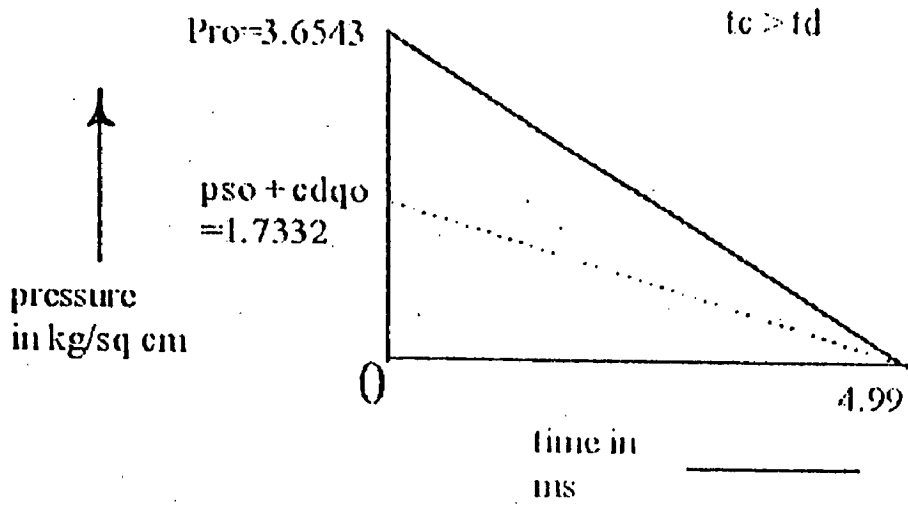


FIG 2.10 FRONT FACE LOADING

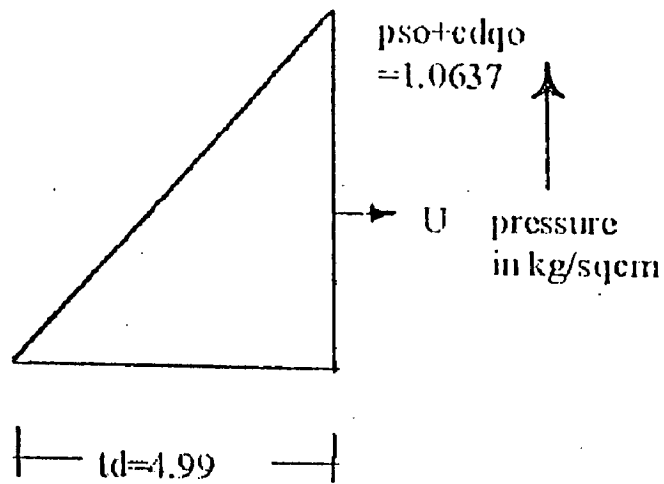


FIG 2.11 ROOF LOADING

# CASE C : 10 KG EXPLOSIVE AT 5 M DISTANCE

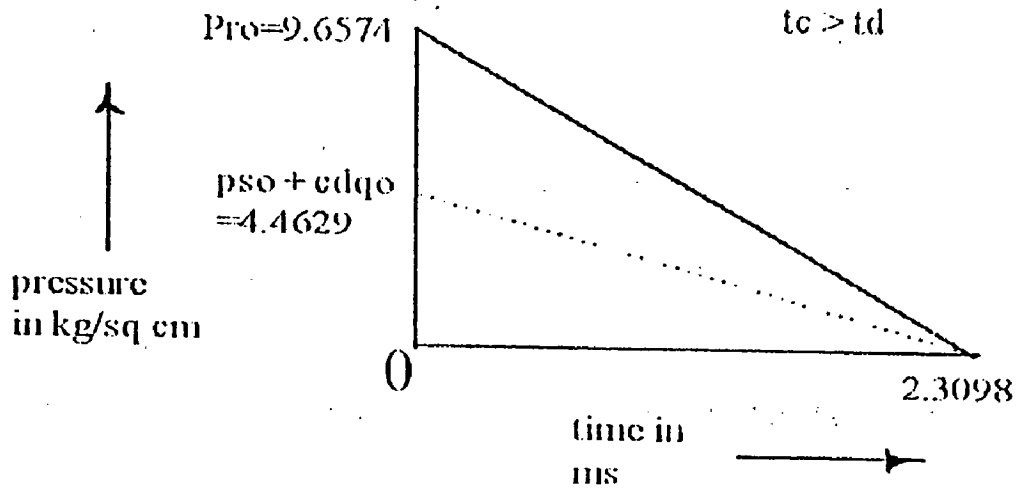


FIG 2.12 FRONT FACE LOADING

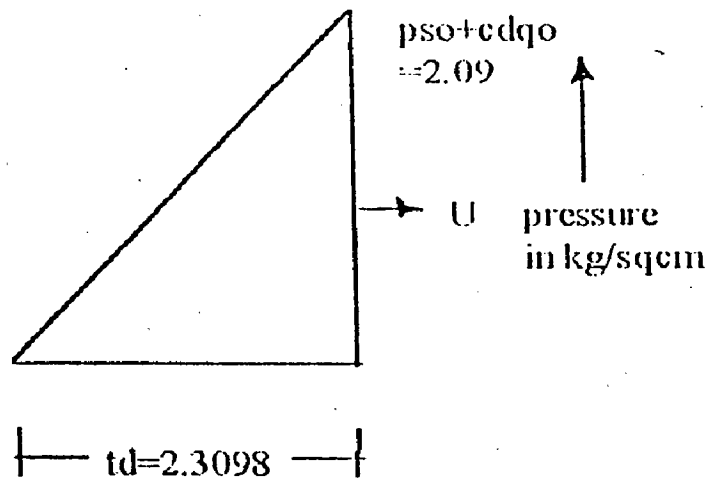


FIG 2.13 ROOF LOADING

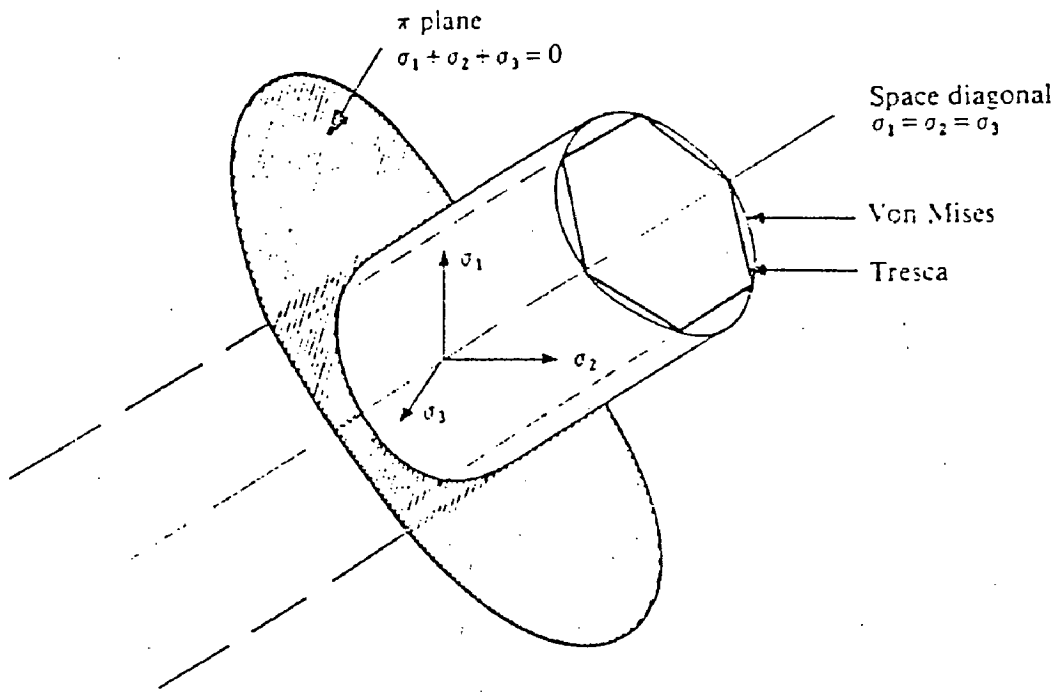


Fig. 4.1 Geometrical representation of the Tresca and Von Mises yield surfaces in principal stress space

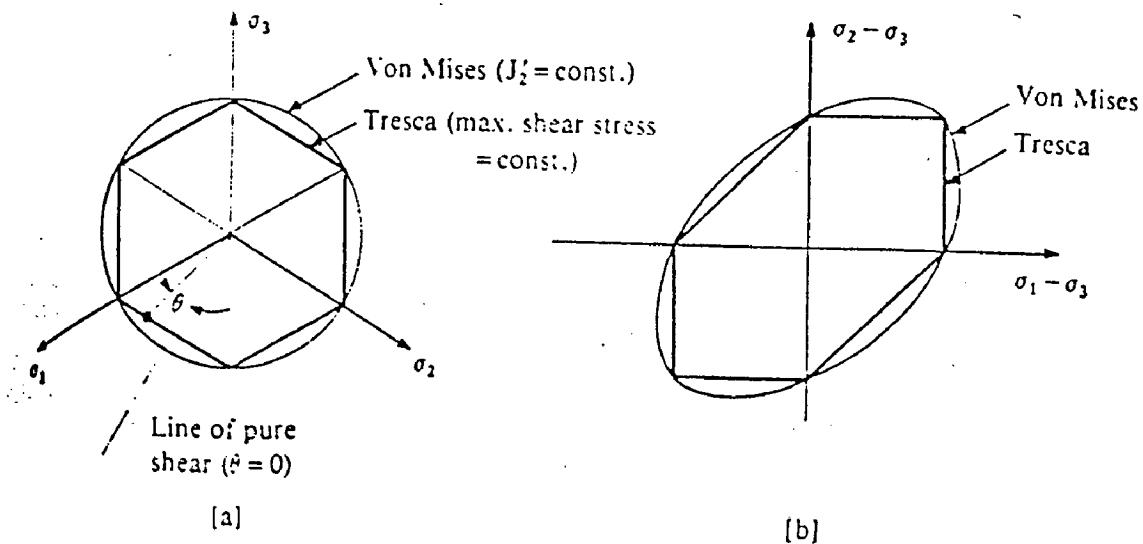


Fig. 4.2 Two-dimensional representations of the Tresca and Von Mises yield criteria (a)  $\pi$  plane representation (b) Conventional engineering representation

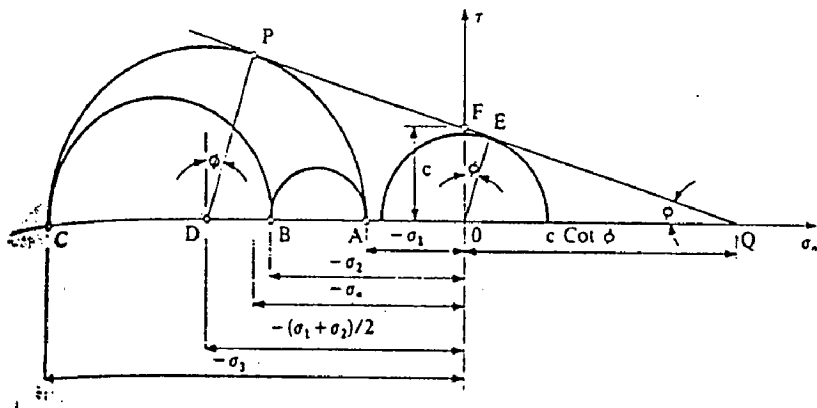


Fig. 4.3 Mohr circle representation of the Mohr-Coulomb yield criterion.

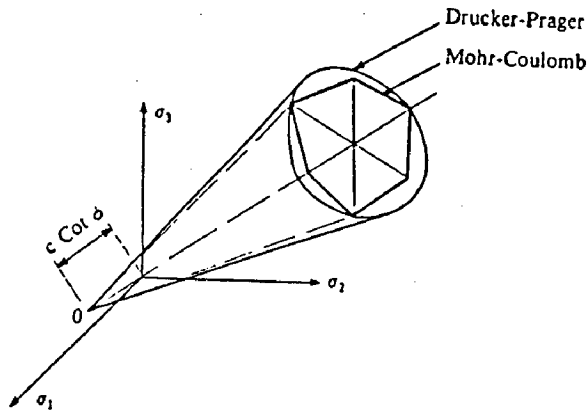


Fig. 4.4(a) Geometrical representation of the Mohr-Coulomb and Drucker-Prager yield surfaces in principal stress space

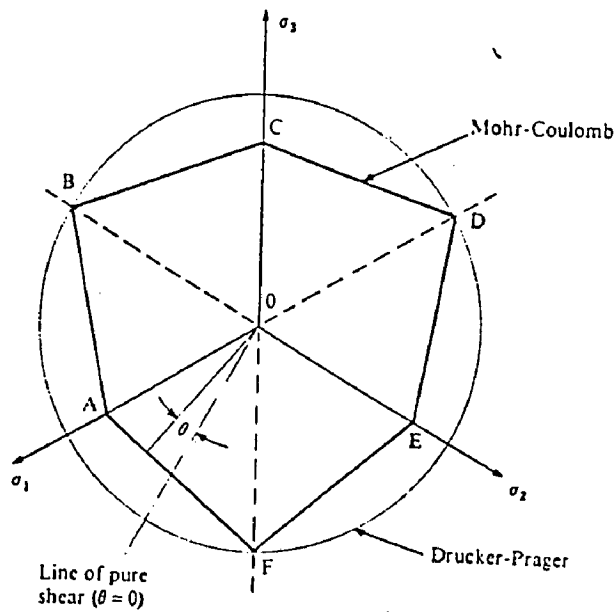


Fig. 4.4(b) Two-dimensional, Pi-plane, representation of the Mohr-Coulomb and Drucker-Prager yield criteria. 62



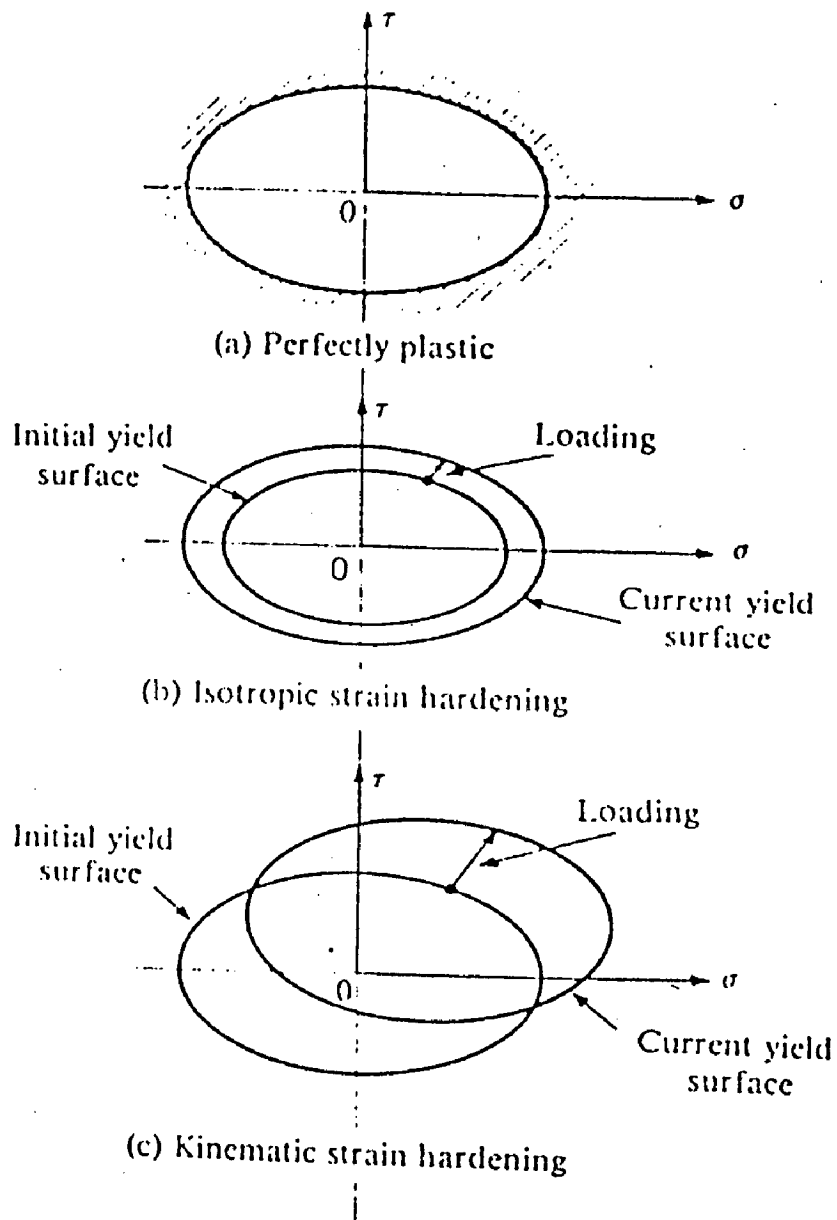


Fig. 4.5 Mathematical models for representation of strain hardening behaviour

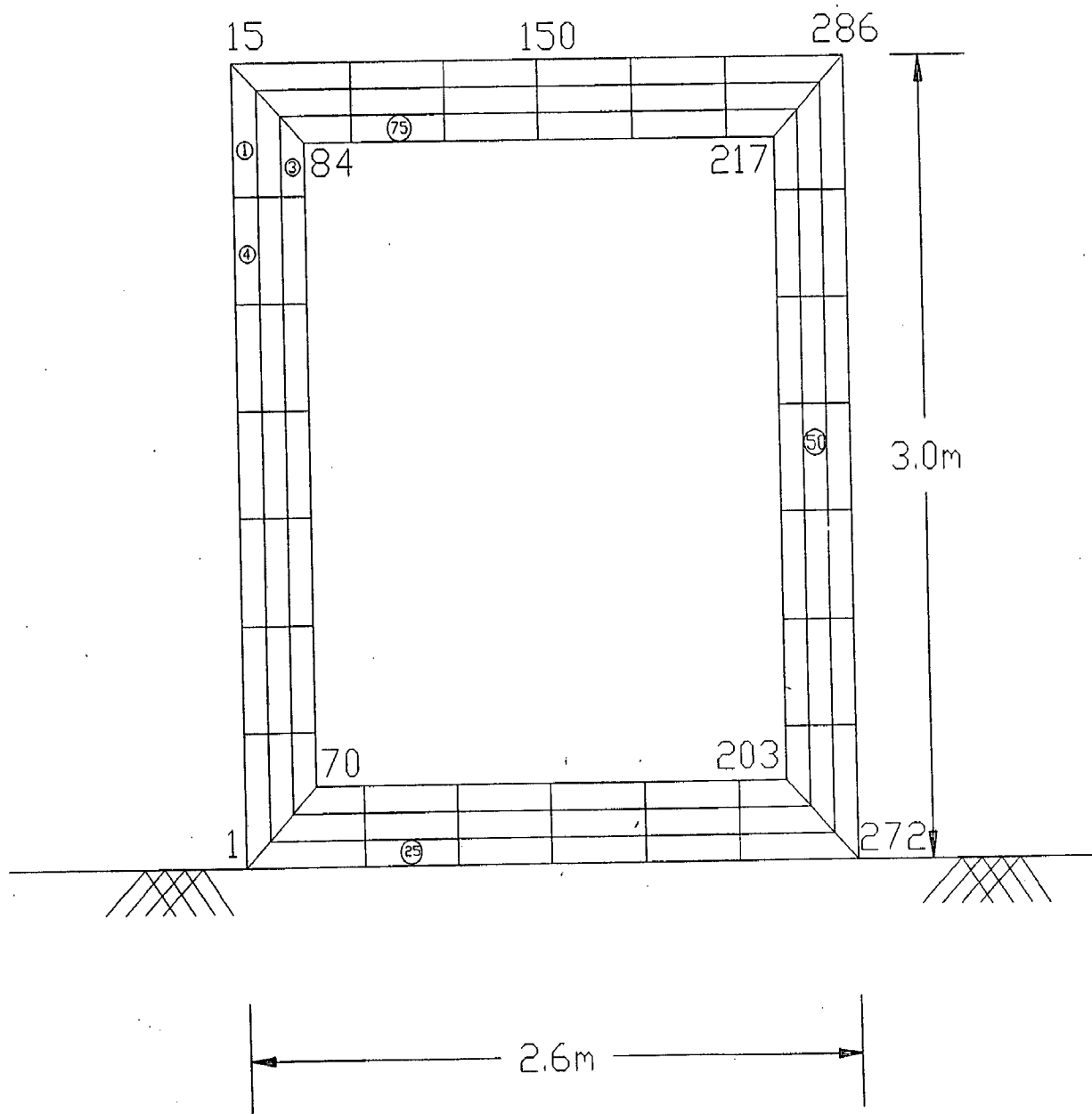


FIG. 5.1 ABOVE GROUND BUNKER

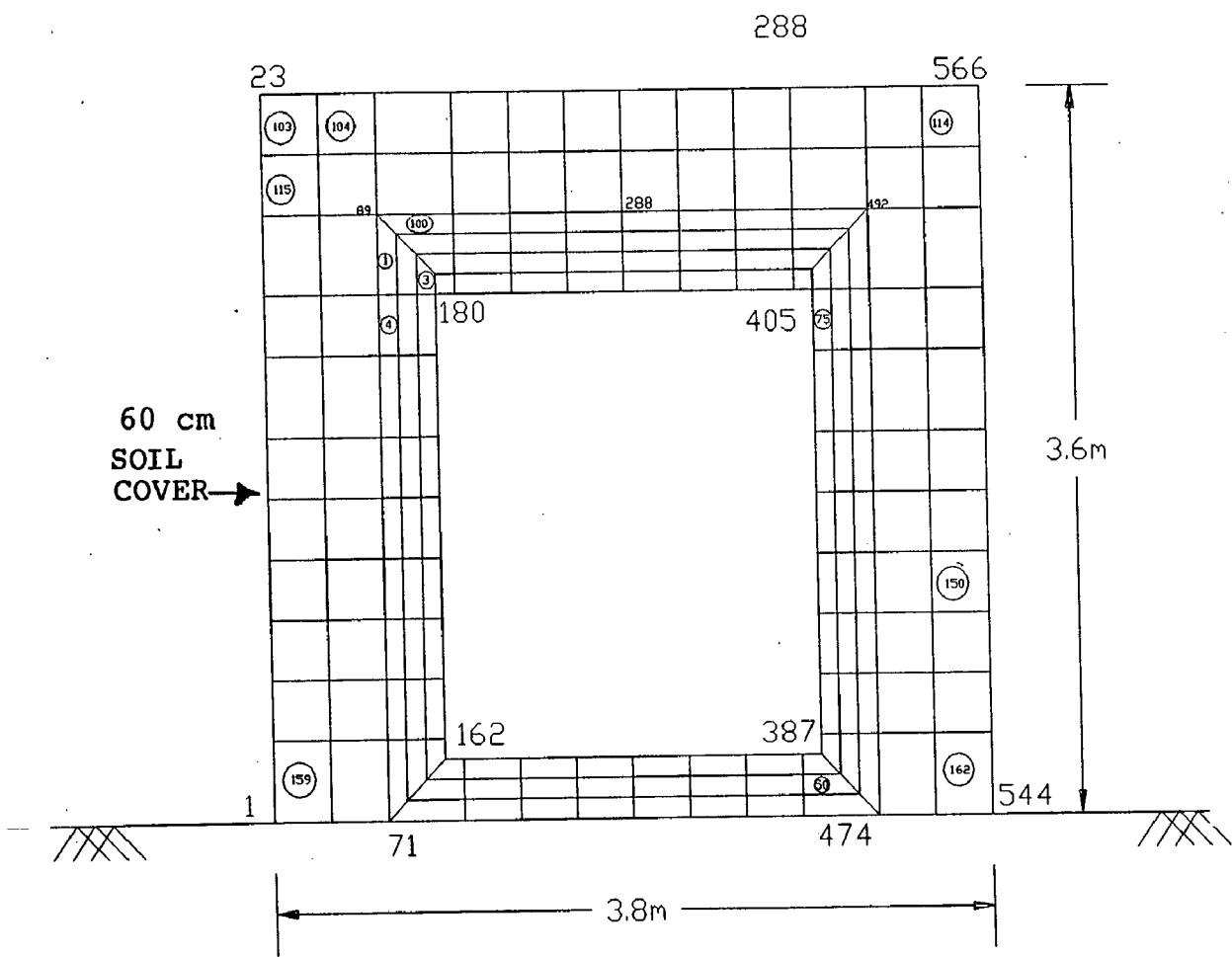


FIG. 5.2 ABOVE GROUND BUNKER WITH SOIL COVER

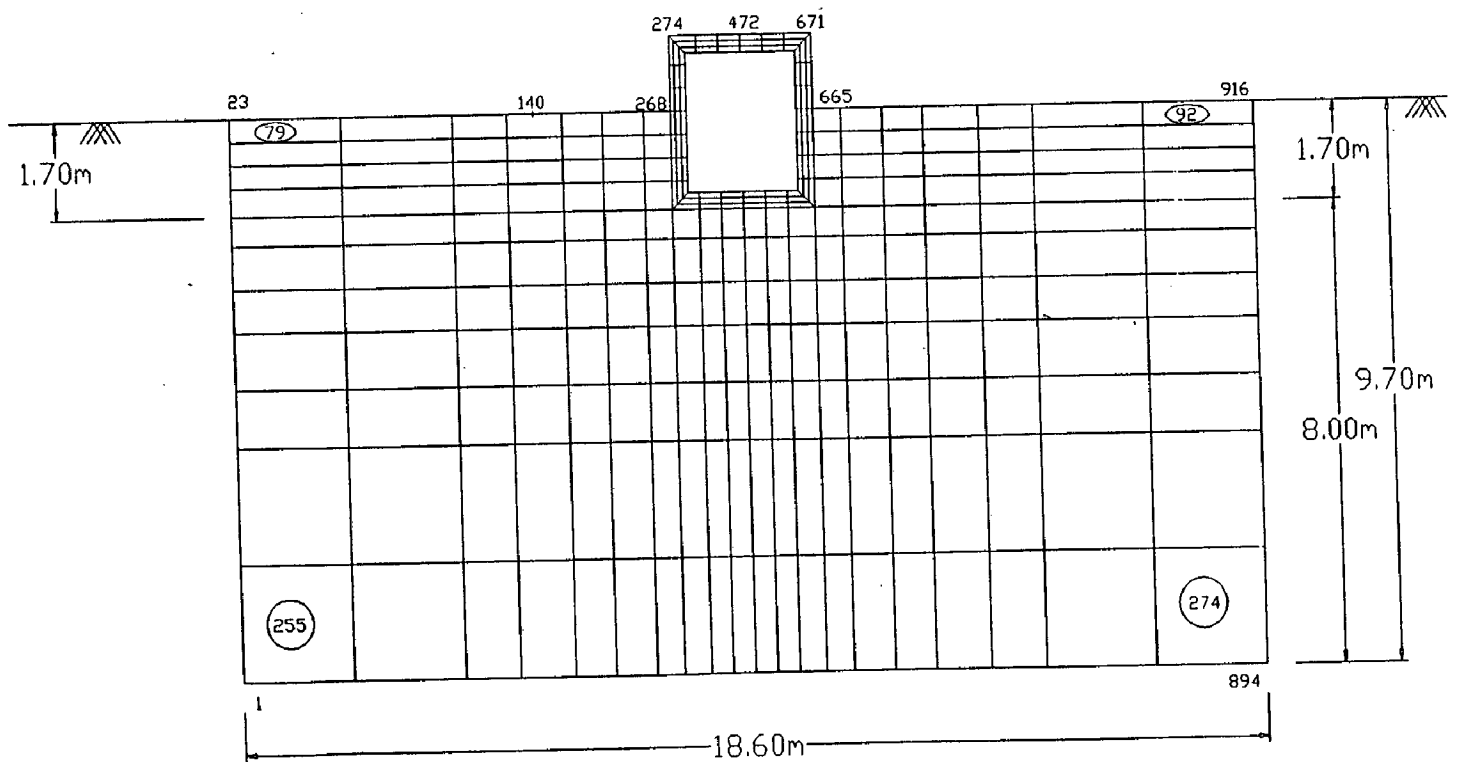


FIG. 5.3 SEMI-BURIED BUNKER

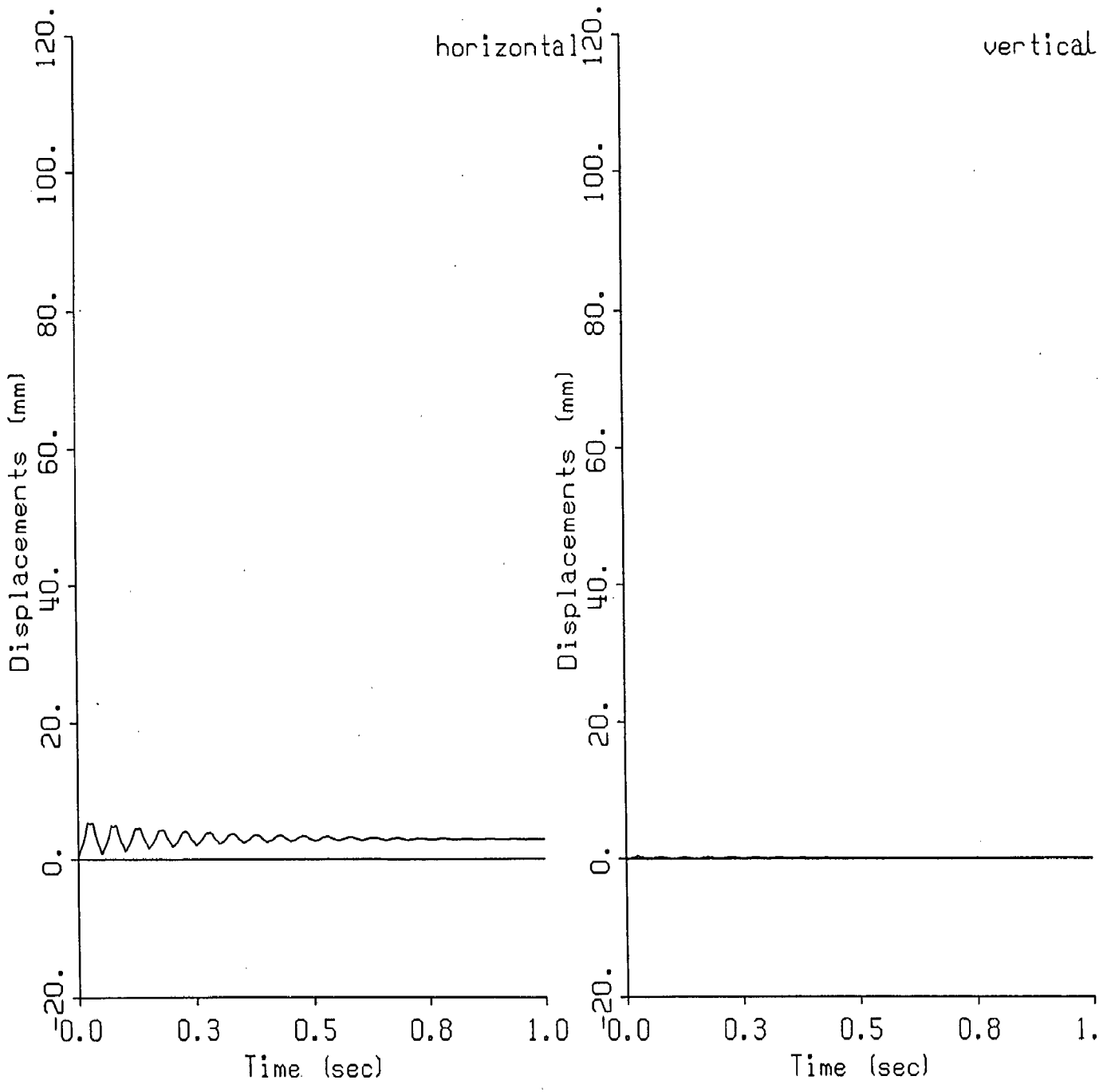


Fig 5.4 Response of an above ground Bunker for 100 kg explosive at 20 m distance

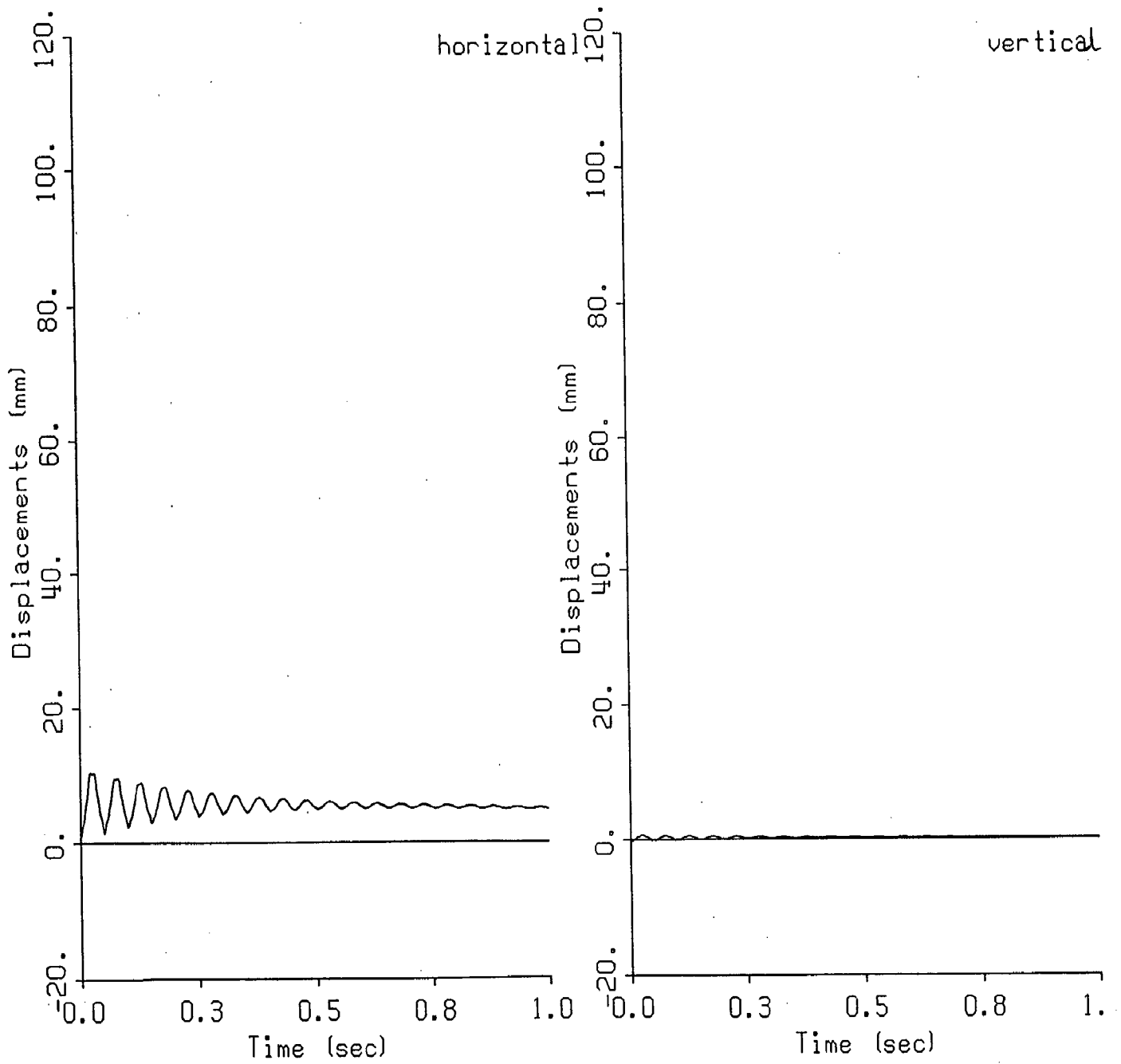


Fig 5.5 Response of an above ground Bunker for 30 kg explosive at 10 m distance

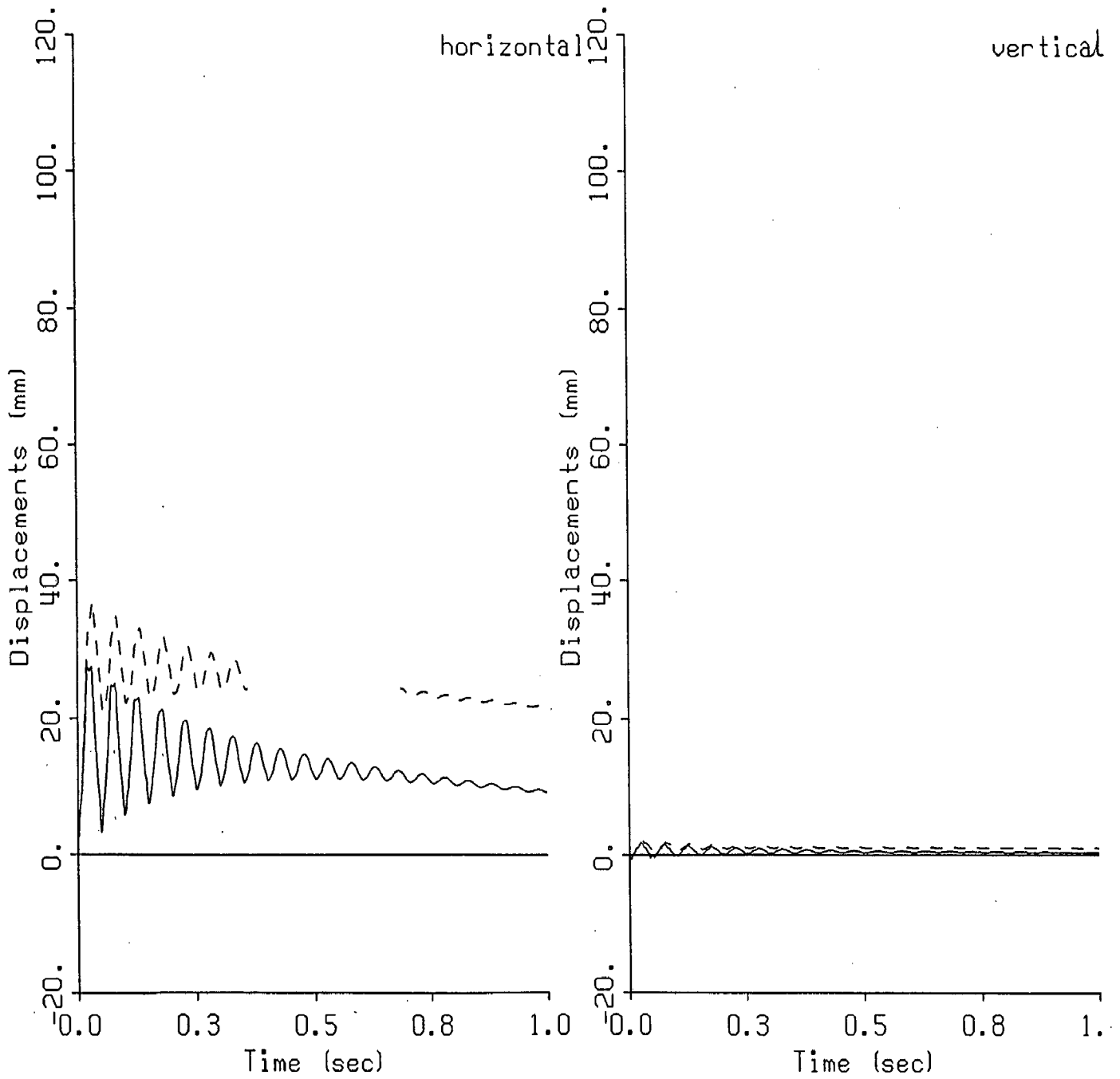


Fig 5.6 Response of an above ground Bunker for 10 kg explosive at 5 m distance

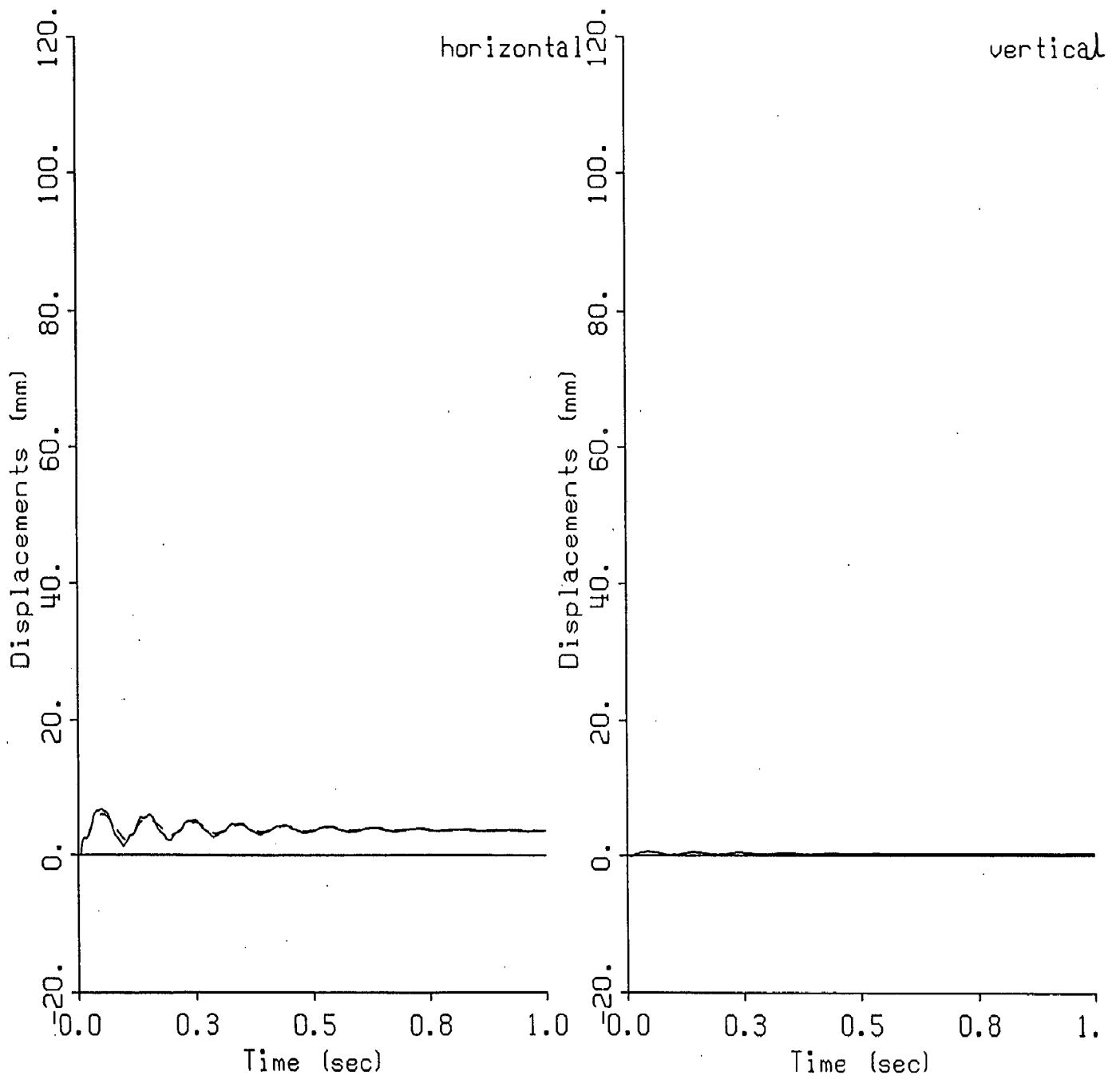


Fig 5.7 Response of an above ground Bunker with soil cover for 100 kg explosive at 20 m distance



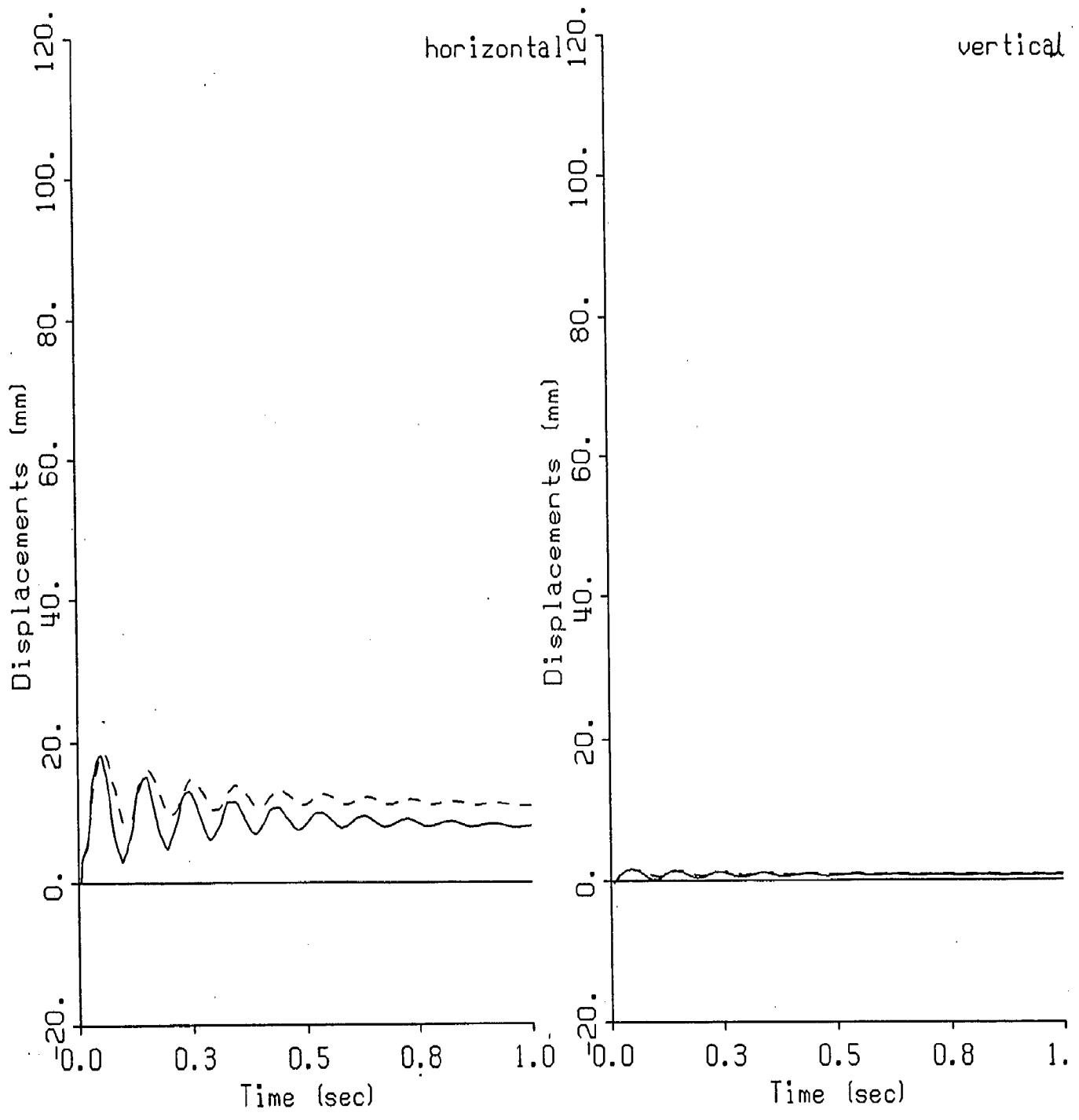


Fig 5.8 Response of an above ground Bunker with soil cover for 30 kg explosive at 10 m distance

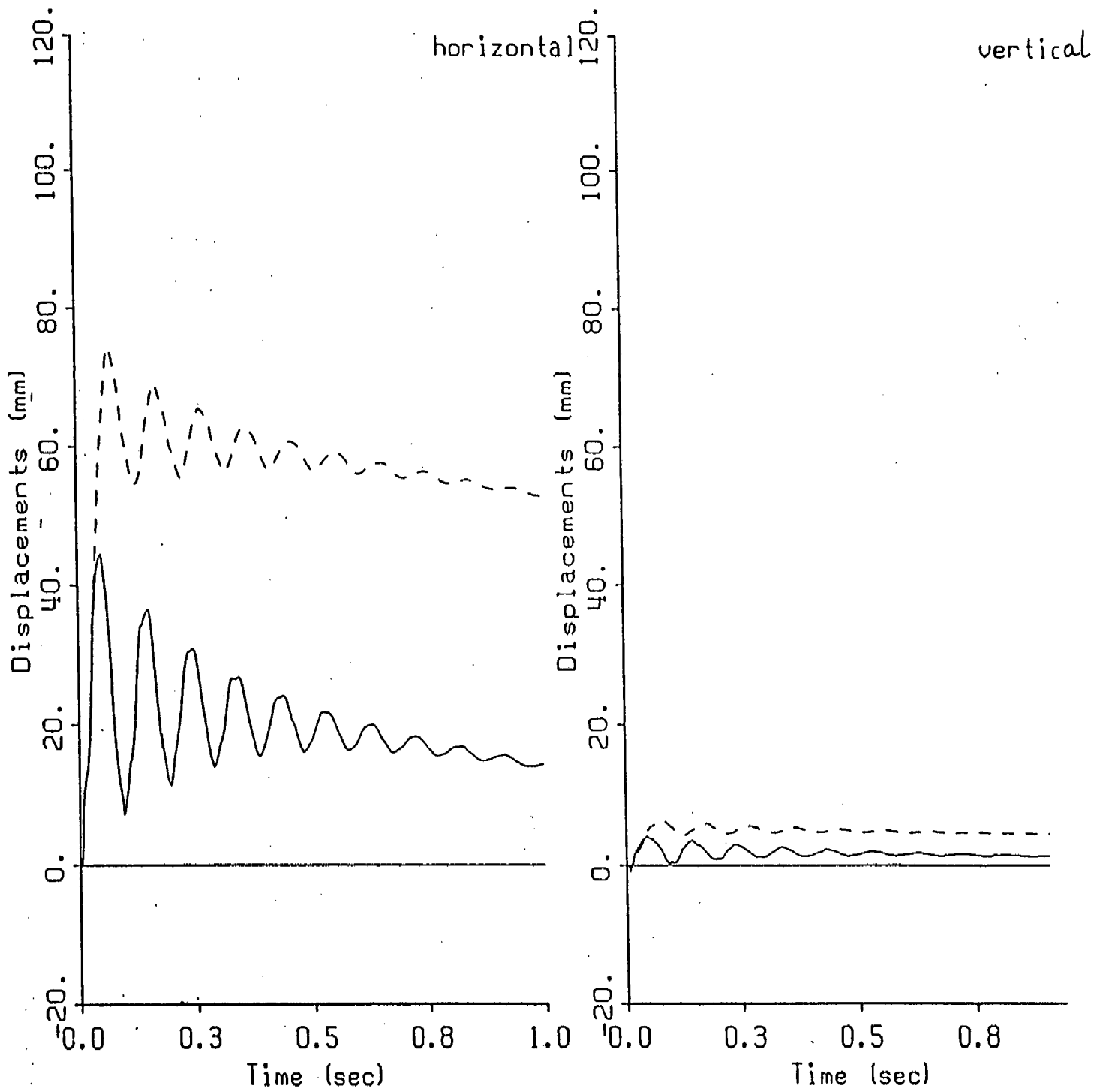


Fig 5.9 Response of an above ground Bunker with soil cover for 10 kg explosive at 5 m distance

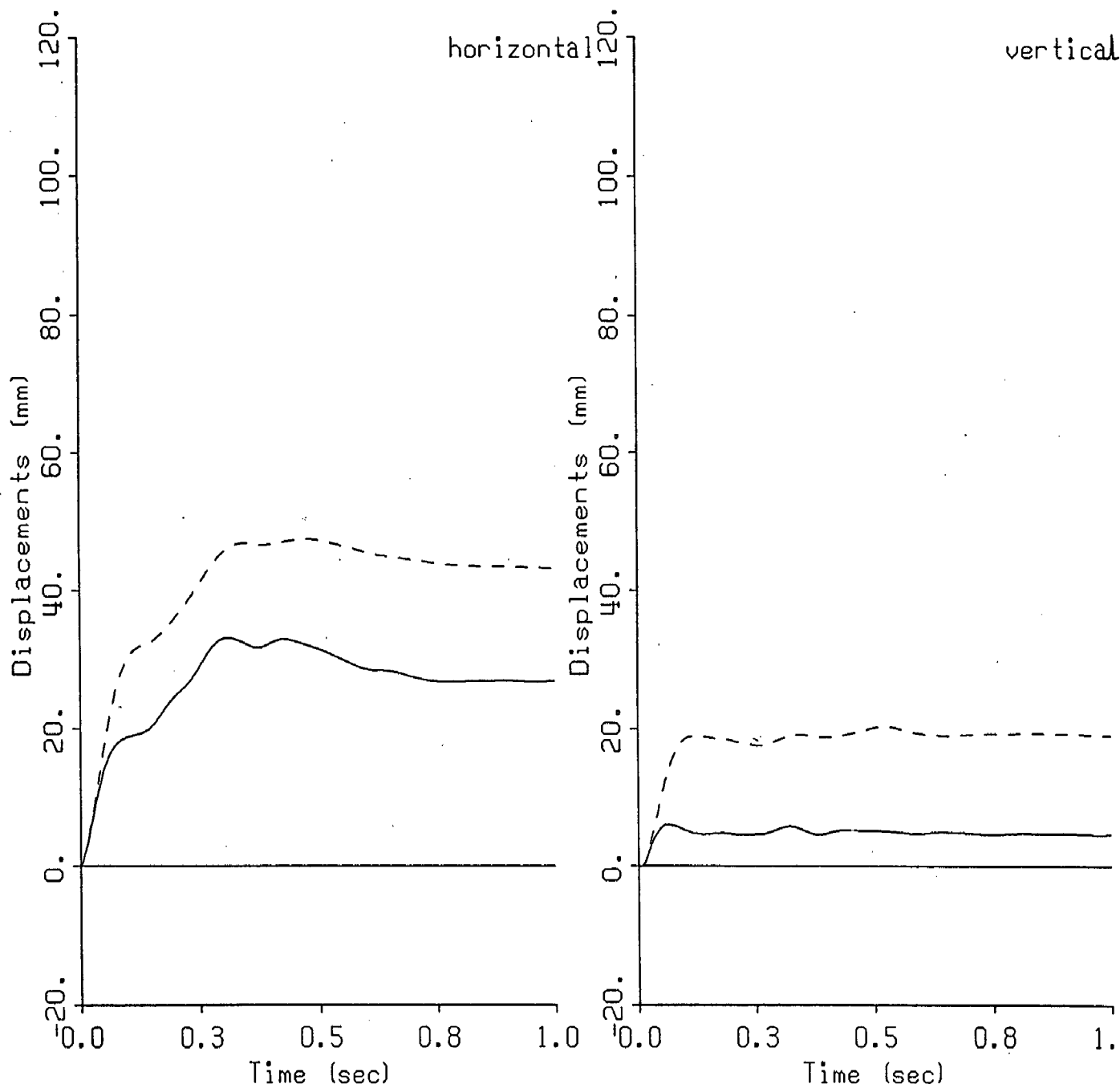


Fig 5.10 Response of a semi-buried Bunker for 100 kg explosive at 20 m distance

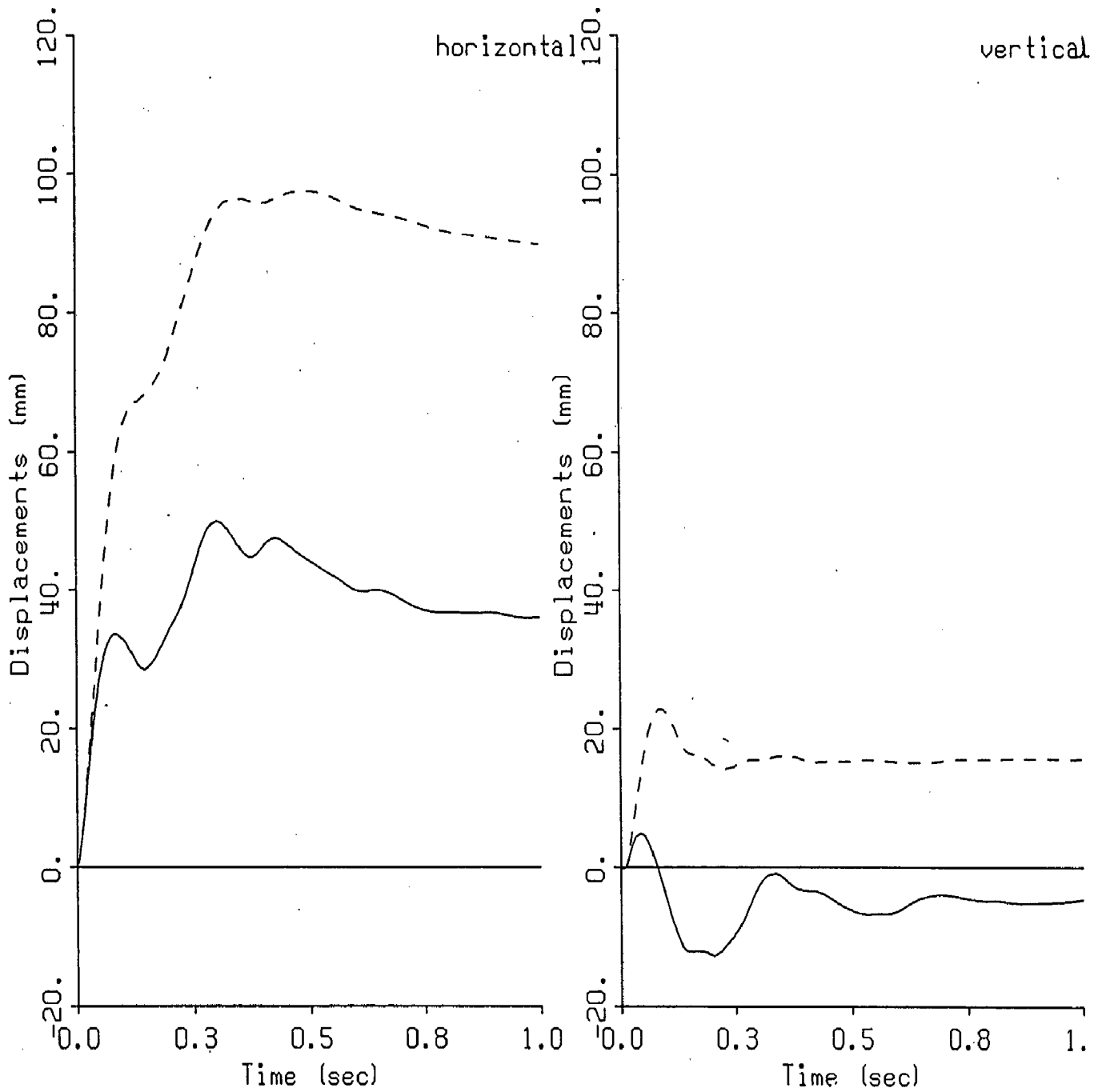


Fig 5.11 Response of a semi-buried Bunker for 30 kg explosive at 10 m distance

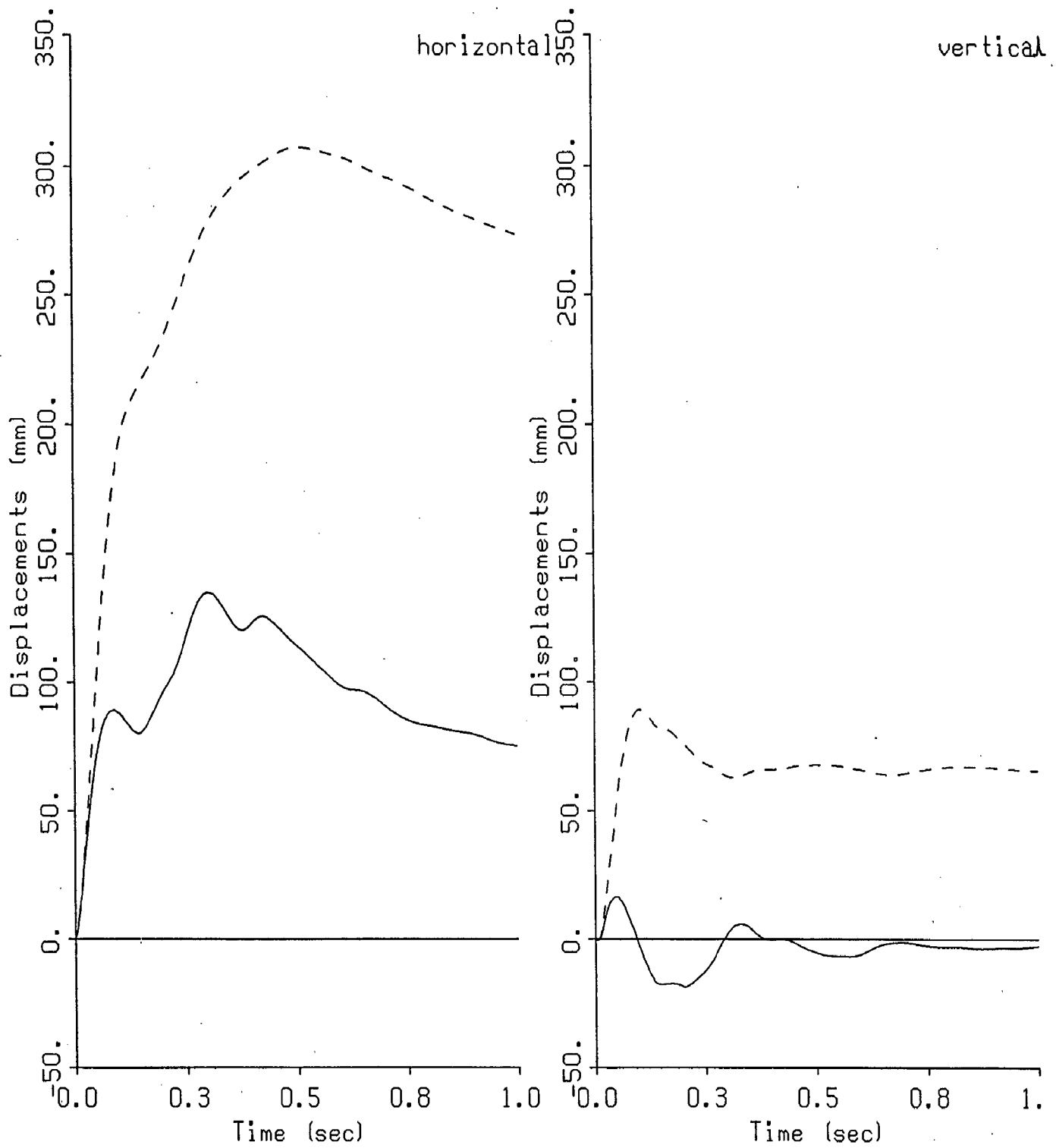
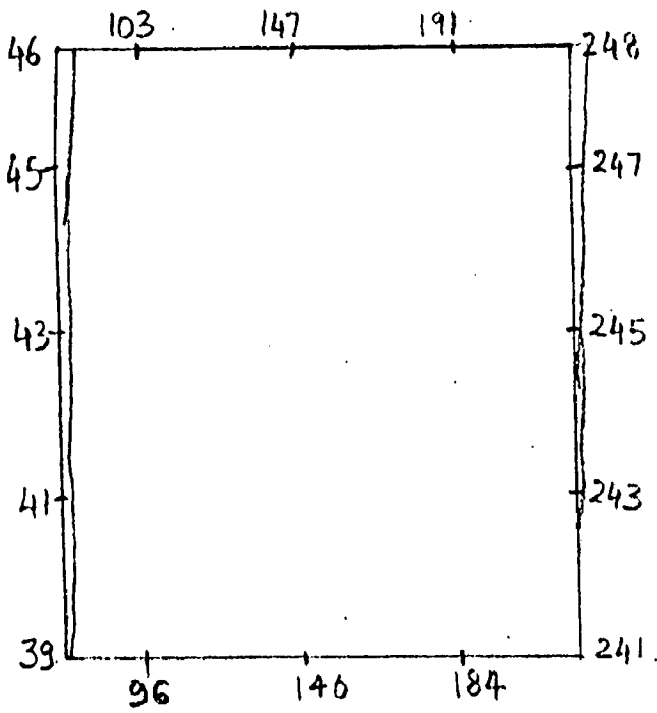
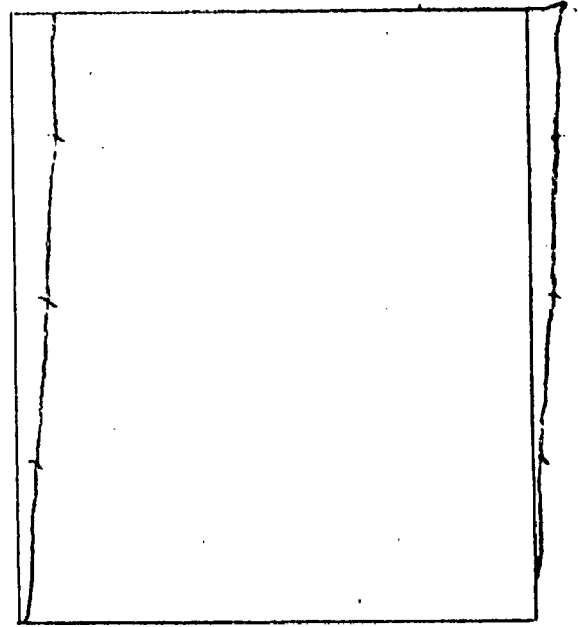


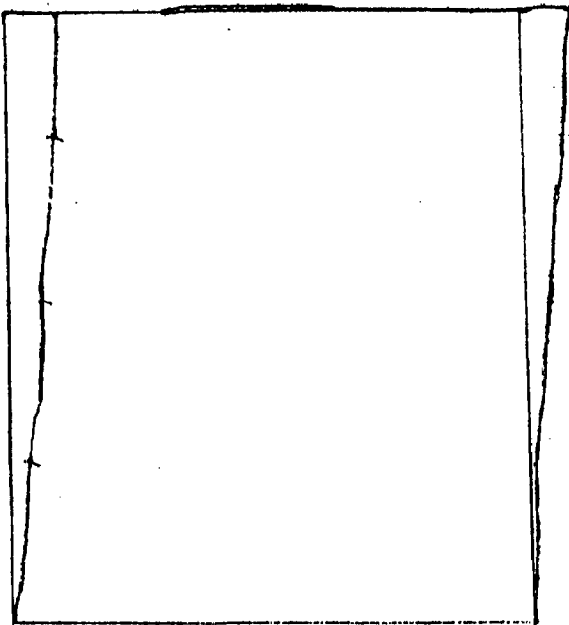
Fig 5.12 Response of a semi-buried Bunker for 10kg explosive at 5m distance



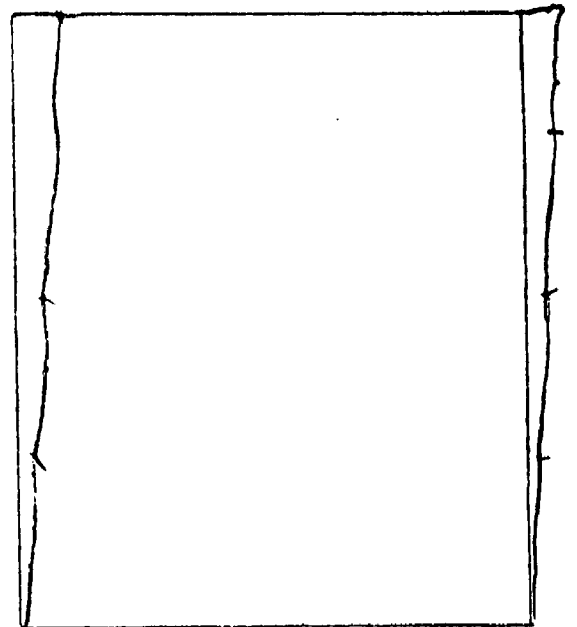
(a) AT 10 ms



(b) AT 20 ms

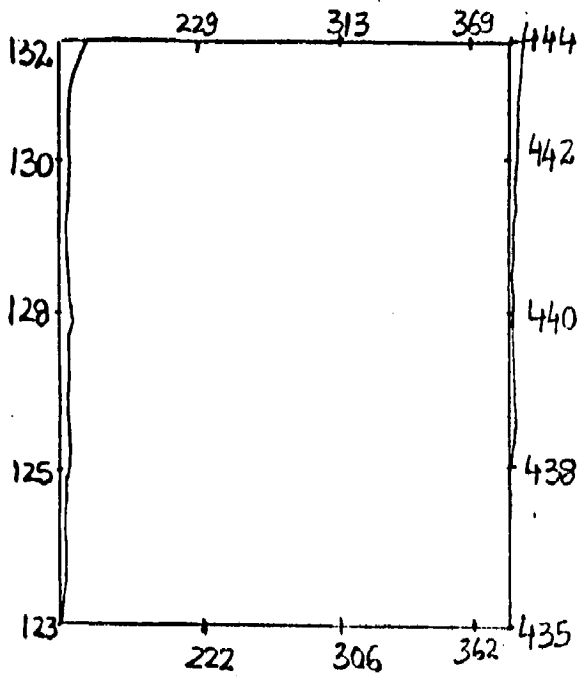


(c) AT 40 ms

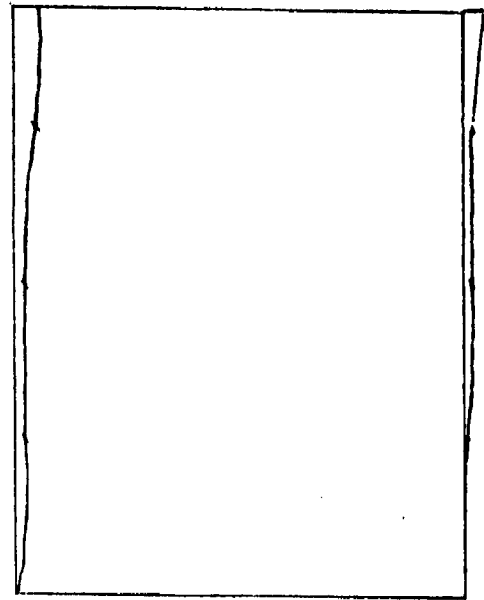


(d) AT 100 ms

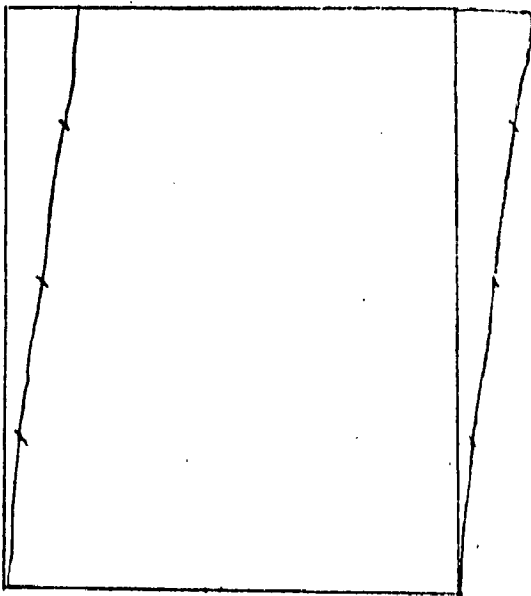
FIG. 5.13 Deflected profile of an above ground bunker at various time intervals



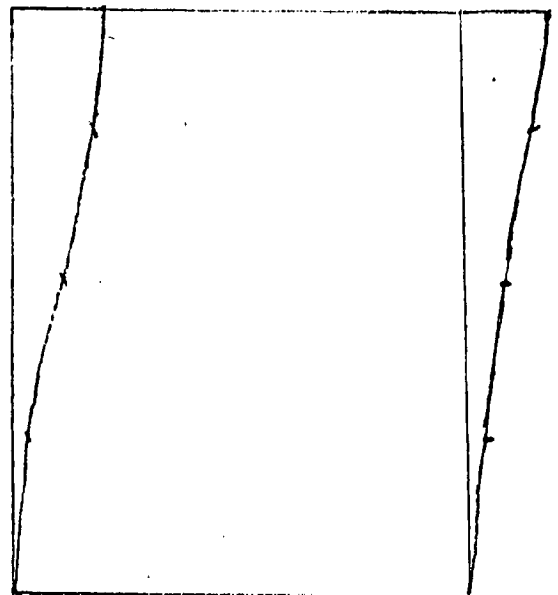
(a) AT 10 ms



(b) AT 20 ms

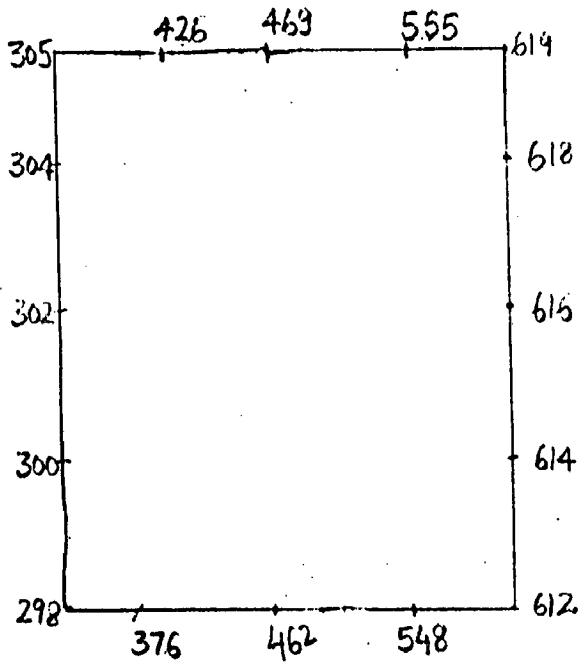


(c) AT 40 ms

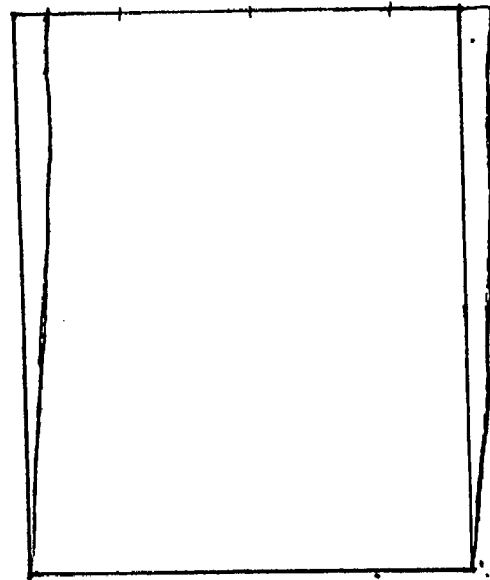


(d) AT 100 ms

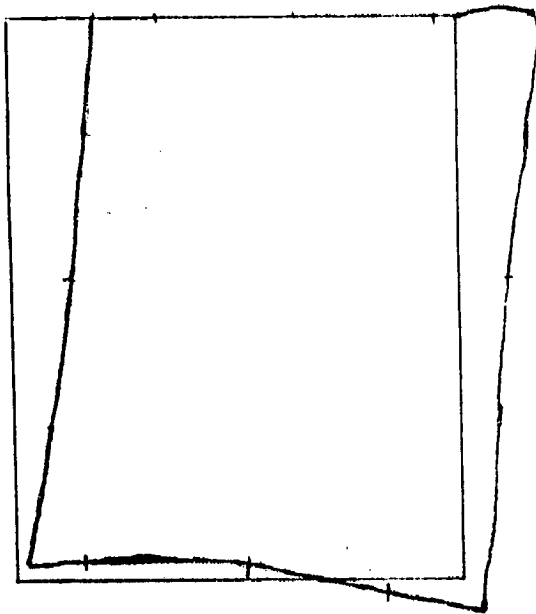
FIG. 5.14 Deflected profile of an above ground bunker with soil cover at various time intervals.



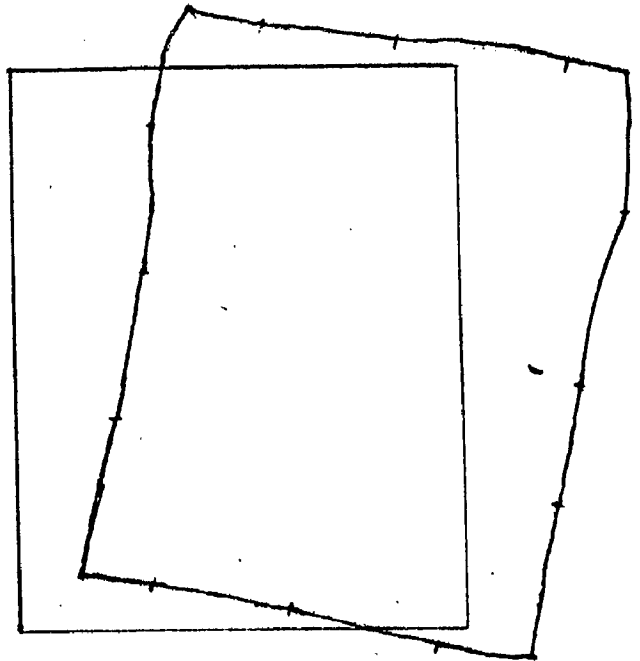
(a) AT 10 ms



(b) AT 20 ms



(c) AT 40 ms



(d) AT 100 ms

FIG. 5.15 Deflected profile of a semi-buried bunker at various time intervals.



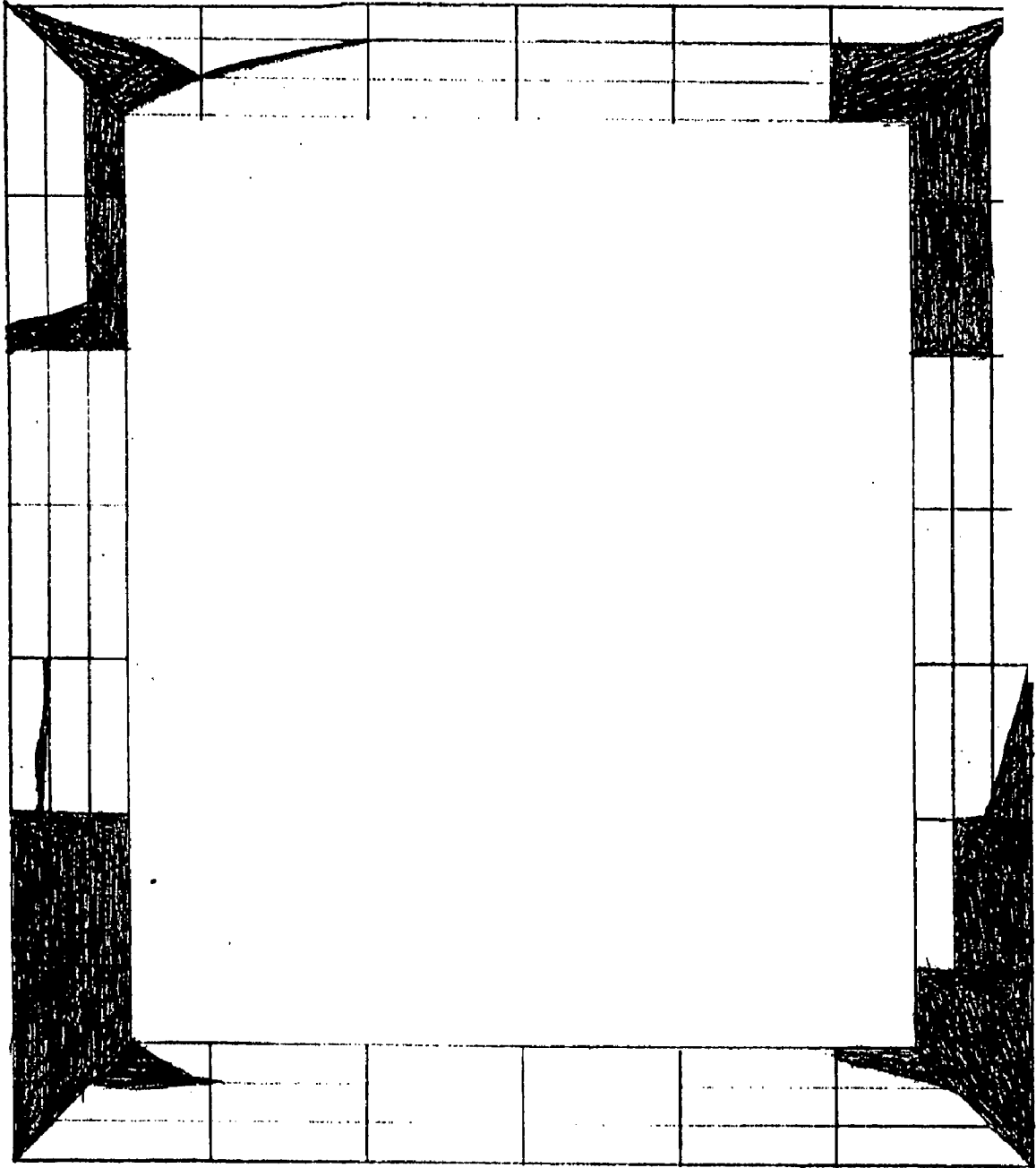


FIG. 5.16 Yielded profile of an above ground bunker.

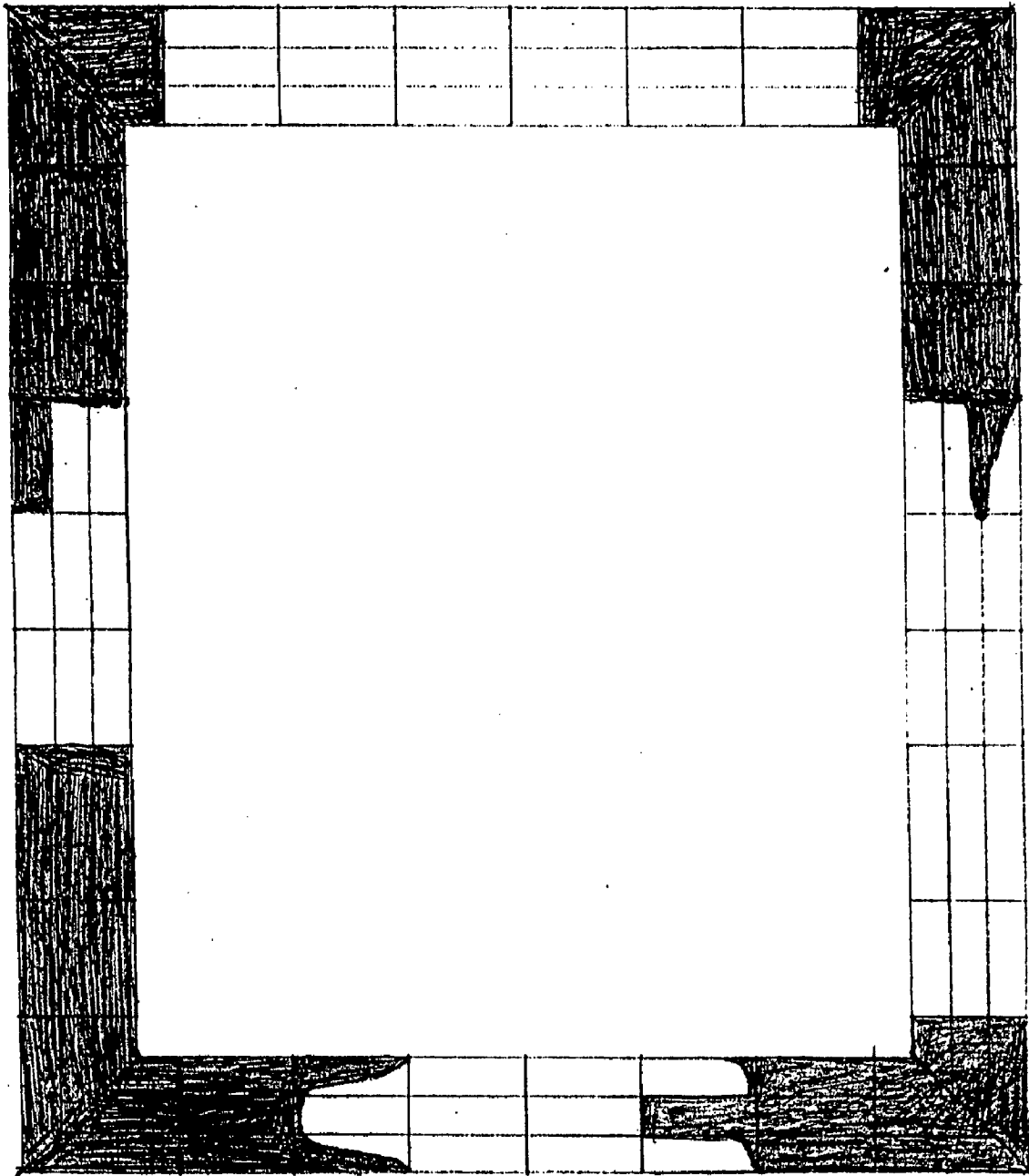


FIG. 5.17 Yielded profile of an above ground bunker with soil cover.



**Table 2.1 Blast Parameters from Ground Burst of 1 Tonne Explosive**

Distance m x	Peak Side on over- pressure ratio $P_{s0}/P_a$	Mach No. M	Positive phase duration $t_0$ , milli- secs	Duration of equivalent triangular pulse $t_d$ , milli-secs	Dynamic pressure ratio $q_0/P_a$	Peak Reflected overpre- ssure ratio $P_{r0}/P_a$
1	2	3	4	5	6	7
15	8.00	2.80	9.50	5.39	10.667	41.60
18	5.00	2.30	11.00	7.18	5.208	20.50
21	3.30	1.96	16.38	9.33	2.643	12.94
24	2.40	1.75	18.65	11.22	1.532	8.48
27	1.80	1.60	20.92	13.30	0.920	5.81
30	1.40	1.48	22.93	15.39	0.583	4.20
33	1.20	1.42	24.95	16.31	0.439	3.45
36	1.00	1.36	26.71	17.94	0.312	2.75
39	0.86	1.32	28.22	19.20	0.235	2.28
42	0.76	1.28	29.74	20.22	0.186	1.97
45	0.66	1.25	31.25	21.60	0.142	1.66
48	0.59	1.23	32.26	22.70	0.115	1.46
51	0.53	1.20	33.52	23.70	0.093	1.28
54	0.48	1.19	34.52	24.70	0.077	1.14
57	0.43	1.17	35.53	26.40	0.062	1.01
60	0.40	1.16	36.29	26.60	0.054	0.93
63	0.37	1.15	37.30	27.80	0.046	0.85
66	0.34	1.14	38.05	28.76	0.039	0.77
69	0.32	1.13	38.81	29.25	0.035	0.72
72	0.30	1.12	39.56	29.87	0.031	0.67
75	0.28	1.11	40.32	30.71	0.027	0.62
78	0.26	1.104	40.82	31.85	0.023	0.58
81	0.25	1.100	41.58	31.92	0.022	0.55
84	0.24	1.095	42.34	32.00	0.020	0.53
87	0.23	1.095	42.84	32.26	0.018	0.50
90	0.22	1.086	43.60	33.39	0.016	0.47
93	0.20	1.082	44.33	34.70	0.014	0.43
96	0.19	1.077	45.46	35.37	0.013	0.41
99	0.18	1.072	45.61	36.22	0.012	0.40

Note 1 - The value of  $p_a$  the ambient air pressure may be taken as 1 kg/cm<sup>2</sup> at mean sea level.

**TABLE 5.1 : MATERIAL PARAMETERS**

Sl NO.	PARTICULARS	CONCRETE	SOIL
1	Young's Modulus, E in $\text{N/m}^2$	$2.15 \times 10^{10}$	$2.00 \times 10^7$
2	Poisson's Ratio, $\nu$	0.20	0.35
3	Thickness for Plane Stress Problem, t	0.00	0.00
4	Mass Density per Unit Volume, $\rho$ in $\text{kg/m}^3$	2500	1800
5	Temperature Co-efficient, $\alpha_t$	0.00	0.00
6.	Reference Yield Value, $F_0$ in $\text{N/m}^2$	$2.00 \times 10^7$	$0.25 \times 10^5$
7.	Hardening Parameter, $H'$ in $\text{N/m}^2$	$2.15 \times 10^9$	$2.00 \times 10^6$
8.	Friction Angle, $\phi$ in Degrees	0.00	$28^\circ$

## REFERENCES

1. Baker W.E. (1980), "A Manual for the Prediction of Blast and Fragment loadings on Structures", US Department of Energy, Texas, USA.
2. Biggs J.M. (1964), "Introduction to Structural Dynamics", McGraw-Hill Book Company, New York.
3. Cook R.D. (1974), "Concepts and Applications of Finite Element Analysis", John Wiley and Sons Inc..
4. Hussain Abbas (1992), "Dynamic Response of Structures Subjected to Missile Impact", Ph.D. Thesis, Department of Civil Engineering, University of Roorkee, Roorkee.
5. IS:4991-1968, "Indian Standard Criteria for Blast Resistant Design of Structures for Explosions above Ground", ISI, New Delhi.
6. Kinney G.F. and Graham K.J. (1985), "Explosive Shocks in Air", Springer-Verlag, Newyork Inc..
7. Mathur Vivek Capt. (1995), "Computer Aided Design of RCC Box Type Structures for Blast Loadings", ME Thesis, Department of Civil Engineering, University of Roorkee, Roorkee.
8. Owen D.R.J. and Hinton E. (1986), "Finite Elements in Plasticity: Theory and Practice" Pineridge Press Limited, Swansea, UK.
9. Srivastava Maj. A.K. (1990), "Blast Resistance and Shatter Proof Properties of Composite Elements", ME Thesis, Department of Civil Engineering, University of Roorkee, Roorkee.
10. Stevens D.J. and Krauthammer T. (1991), "Analysis of Blast Loaded, Buried RC Arch Response, Part I: Numerical Approach", J. Struct. Engg., ASCE, 117(1), 197-212.

11. Stevens D.J. and Krauthammer T. (1991), "Analysis of Blast Loaded, Buried RC Arch Response II: Application", J. Struct. Engg., ASCE, 117(1), 213-234.
12. Thanoon Waleed Abdul Malik (1993), "Inelastic Dynamic Analysis of Concrete Frames under non-nuclear Blast Loadings", Ph.D. Thesis, University of Roorkee, Roorkee.
13. US Army Corps of Engineers, TM-5-1300(1969), "Structures to Resist the Effect of Accidental Explosions", Vol. I.
14. US Army Armament Research and Development Centre, ARLCD-SP-84001 (1986), "Structures to Resist the Effects of Accidental Explosions", Vol. II - Blast, Fragment and Shock Loads.
15. Zienkiewicz O.C. and Taylor R.L. (1991) "The Finite Element Method", Vol. I and II, McGraw Hill Books Co., Newyork.